



# Plateau's rotating drops and rotational figures of equilibrium



Jeffrey Elms<sup>a</sup>, Ryan Hynd<sup>b,\*</sup>, Roberto Lopez<sup>c</sup>, John McCuan<sup>c,\*</sup>

<sup>a</sup> Google, 1600 Amphitheatre Parkway, Mountain View, CA 94043, United States

<sup>b</sup> Department of Mathematics University of Pennsylvania, 209 South 33rd St., Philadelphia, PA 19104, United States

<sup>c</sup> School of Mathematics, Georgia Tech, 686 Cherry St, Atlanta, GA 30332, United States

## ARTICLE INFO

### Article history:

Received 28 February 2015

Available online 24 August 2016

Submitted by P. Yao

### Keywords:

Rotating drops

Mean curvature

Plateau

Delaunay

## ABSTRACT

We give a detailed classification of all rotationally symmetric figures of equilibrium corresponding to rotating liquid masses subject to surface tension. When the rotation rate is zero, these shapes were studied by Delaunay who found six different qualitative types of complete connected interfaces (spheres, cylinders, unduloids, nodoids, catenoids, and planes). We find twenty-six qualitatively different interfaces providing a complete picture of symmetric equilibrium shapes, some of which have been studied by other authors. In particular, combining our work with that of Beer, Chandrasekhar, Gulliver, Smith, and Ross, we conclude that every compact equilibrium is in either a smooth connected one parameter family of spheroids or a smooth connected one parameter family of tori (possibly immersed in either case).

© 2016 Elsevier Inc. All rights reserved.

## 1. Introduction

It is well known that an immiscible liquid drop immersed completely in a homogeneous fluid and isolated from body forces (magnetic, gravitational, etc.) assumes, at rest, the shape of a sphere. This fact was observed by Joseph Plateau in the 1840s while conducting experiments with neutrally buoyant oil drops immersed in a solution of alcohol and water. Plateau observed that such an isolated drop may rigidly rotate and assume an axisymmetric shape [9]. Based on his observations Plateau also conjectured that toroidal equilibrium shapes exist and satisfy an appropriate mathematical equation.

In 1855, August Beer [1] derived a geometric equation modeling the shape of rotationally symmetric rotating drops: The mean curvature of the boundary of the drop is a quadratic function of distance to the axis of rotation. Beer went on to study certain simply connected solutions of his equation. In 1914, Rayleigh [10] obtained sufficient conditions to guarantee the existence of a toroidal solution. In his 1964 paper [3], Chandrasekhar considered the stability of Beer's simply connected rotationally symmetric solutions.

\* Corresponding authors.

E-mail address: rhynd@math.upenn.edu (R. Hynd).

All the work mentioned above involves rotationally symmetric figures, but the geometric condition can also be applied to non-symmetric interfaces. Henry Wente [13] proved that every equilibrium rotating drop has a symmetry plane orthogonal to its axis of rotation, and later Rafael López [8] showed, under certain restrictions, that rotating bubbles must be axially symmetric. However, Brown and Scriven [2] obtained multi-lobed drop shapes numerically as bifurcations from the rotationally symmetric family. Two and three lobed shapes were produced experimentally in the low gravity environment of Spacelab by a group of researchers from JPL [12]. A mathematical proof of existence for specific non-symmetric solutions of the modeling equation bifurcating from the rotationally symmetric solutions is not known. Kapouleas [7] has constructed non-symmetric solutions which share the symmetry of the surfaces obtained by Brown and Scriven but are far from the rotationally symmetric solutions. We note also that Wilkin-Smith [14] obtained an interesting existence result for solutions close to the sphere. These solutions may be non-symmetric, but the proof is non-constructive and apparently does not provide this information. The paper [14] also contains an extensive list of references related to rotating drops.

Plateau's conjecture on the existence of toroidal solutions was unresolved until 1984, when Gulliver [4] verified that toroidal rotating drops do indeed exist. Gulliver found a one parameter family of embedded tori each with convex cross section. Smith and Ross [11], following Gulliver, characterized all embedded toroidal figures of equilibrium. Hynd and McCuan showed in [6] the existence of infinitely many immersed toroidal solutions with figure-eight cross section.

Heine [5] has recently numerically computed non-symmetric toroidal shapes with many lobes. Like the shapes of Brown and Scriven, there is no rigorous mathematical proof that these shapes correspond to solutions of the modeling equation.

In this work, we classify all rotational figures of equilibrium. These include the classical rotating drops studied by Beer, Rayleigh, Chandrasekhar (spheroids), rotating bubbles, and toroidal drops. There are also unbounded solutions and additional immersed solutions which have received little attention in the literature but arise in modeling the interfaces of rotating liquid masses in contact with a rotating container; see Fig. 5. Our classification yields twenty-six qualitatively different shapes. We show that every compact rotational figure of equilibrium is a spheroid or toroidal figure and prove that all of these surfaces belong to two well-defined smooth one parameter families. We believe this work provides a complete picture for the rotationally symmetric equilibrium figures.

### 1.1. Summary of shapes

The complete list of qualitative types of rotational figures of equilibrium includes the Delaunay surfaces (for zero angular velocity) and the twenty-six surfaces we now describe. Perhaps the easiest way to describe the latter shapes is by comparison to the Delaunay surfaces shown in Fig. 1 and as deformations of surfaces in the family itself. We point out, in particular, the qualitative properties of the nodoid, having an immersed periodic meridian that loops toward the axis with no inflections, and the unduloid, having an embedded periodic meridian with one inflection in each half-period.

Circular cylinders (with the same axis as the axis of rotation) are possible solutions with both zero and nonzero angular velocity. These shapes of liquids in rotation are indistinguishable from the shapes of liquid cylinders at rest. Every possible radius is represented among the cylinders, and the orientation may be taken in either direction (to model liquid rotating within the cylinder or a cylinder enclosed by rotating liquid).

There are also solutions that are qualitatively the same as Delaunay unduloids; see Fig. 2(a). To denote the fact that these surfaces are analytically distinct from unduloids, we refer to them as *unduloid type*. In the case of zero angular velocity, i.e., the surfaces of Delaunay, the unduloids are often viewed as smooth deformations of cylinders under which necks and bulges appear. The unduloid type surfaces, for nonzero angular velocity, may also be viewed as deformations of cylindrical solutions.

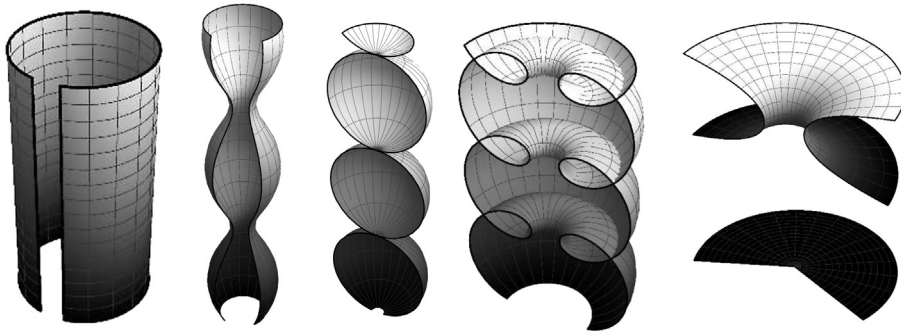


Fig. 1. There is a two parameter family of Delaunay surfaces having six distinct qualitative types: cylinder, unduloid, sphere, nodoid, catenoid, plane. Each surface has constant mean curvature and is rotationally symmetric. We note that the cylinder may be smoothly deformed, within the family of Delaunay surfaces, to an unduloid by the introduction of periodic necks and bulges. Other deformations among these surfaces are possible as well.

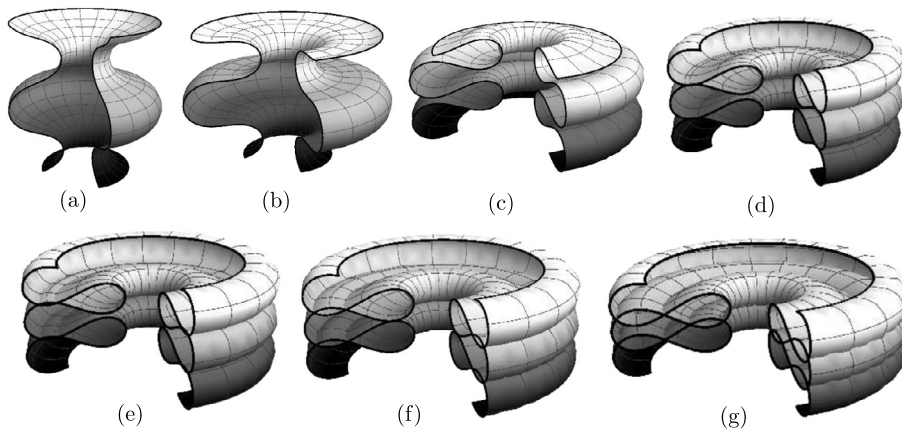


Fig. 2. (a) Unduloid type, (b) breaking unduloid (horizontal tangent), (c) puzzle type (embedded), (d) puzzle type (immersed with the outer corrugations coming together along a circle of self-tangency), (e) puzzle type (immersed with a higher degree of immersion on the outer corrugations but with the inner corrugations still disjoint), (f) puzzle type (inner corrugations coming together along a circle of self-tangency), and (g) puzzle type (both inner and outer corrugations having a higher degrees of immersion).

It is not possible for a deformation through Delaunay unduloids to produce a meridian which does not project simply onto the axis of rotation. There are no such unduloids. Among the equilibria corresponding to nonzero angular velocity this is possible. Referring to the direction of the axis as vertical, we obtain deformations which resemble an unduloid but have a single horizontal tangent per half-period on the meridian (located at the inflection); see Fig. 2(b). These *breaking unduloids* further deform into surfaces each of which has two horizontal tangents per half period at points distinct from the single inflection; see Fig. 2(c). The resulting meridian is no longer a graph over the axis, and contains corrugations resembling those found on puzzle pieces; we term these surfaces *puzzle unduloids*. While initially embedded for deformations near the breaking unduloid, as one continues the deformation, the corrugations of the puzzle unduloids self-intersect as indicated in Fig. 2 (d–g). The degree of immersion increases until the difference in vertical height between consecutive vertical points on the meridian, later called the *final vertical height of the half period*, is zero. In this way, the periodic puzzle unduloids limit to a countable cover of an immersed figure-eight torus as shown in Fig. 7(a).

The deformation continues through the toroidal solutions to surfaces with fundamentally different qualitative properties. The meridians of these surfaces still have one inflection per half period, but contain immersed loops both toward and away from the axis. For deformations near the figure-eight torus, these *binoids* have a high degree of immersion. Continuing the deformation (which is possible) the loops sepa-

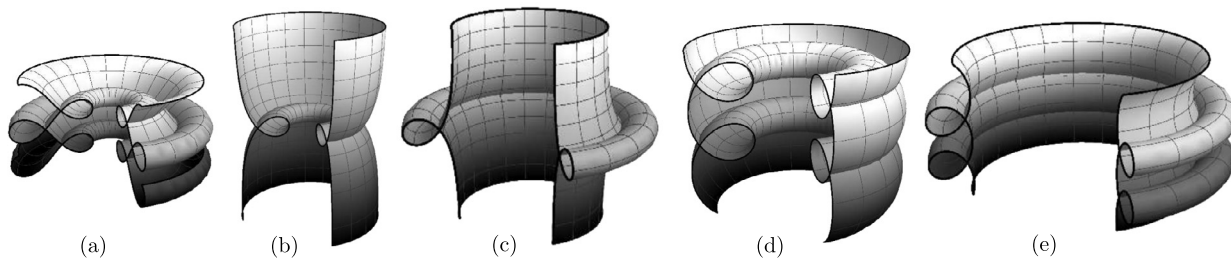


Fig. 3. (a) Binoid, (b) cylindro-nodoid, (c) cylindro-antinodoid, (d) nodoid type, (e) antinodoid.

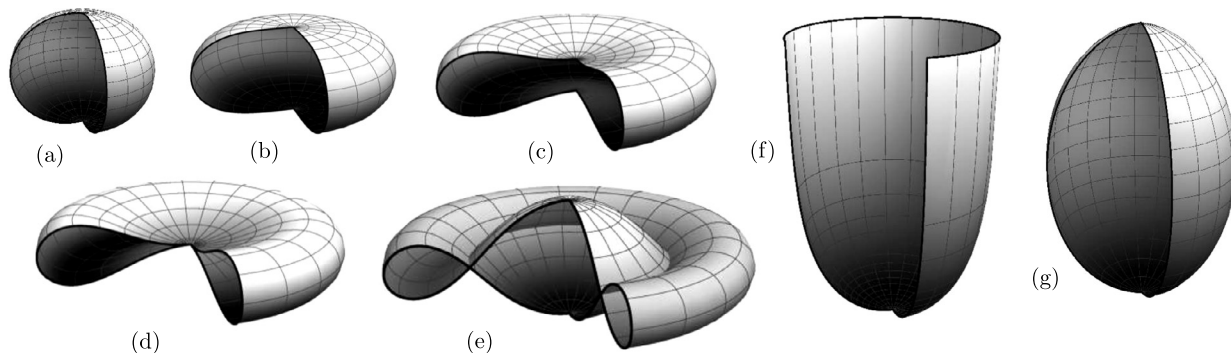


Fig. 4. Generalized spheroids: (a) oblate, (b) flat poled, (c) inflected, (d) pinched, (e) immersed, (f) infinite (half) bubble, (g) prolate spheroid.

rate until there are (on average) only two points of self-intersection per period as indicated on the left in Fig. 3(a).

The deformation continues with the loops spreading farther apart in the vertical direction until, in the limit, two surfaces of distinct qualitative type are obtained. One is asymptotic to a cylinder with a single loop facing inward—a *cylindro-nodoid*. Another is asymptotic to the same cylinder with a single loop facing outward—a *cylindro-antinodoid*. See Fig. 3(b) and (c).

Deformation through the cylindro-nodoid and cylindro-antinodoid is also possible, and each cylindro-nodoid and cylindro-antinodoid is also a limit of surfaces distinct from the binoids discussed above. One family is of *nodoid type*, Fig. 3(d), and the other *antinodoid*, Fig. 3(e). As the names suggest, nodoid type surfaces are qualitatively the same as Delaunay nodoids, though analytically distinct; antinodoid surfaces have inflectionless immersed meridians, but the loops are facing away from the axis.

We turn next to surfaces having contact with the axis of rotation; see Fig. 4. One finds here the oblate (or concave) spheroids considered by Beer and Chandrasekhar, Fig. 4(a). The poles move together under deformation until an inflection point occurs on the axis—the *flat poled spheroid*, Fig. 4(b). Beyond this, the inflection moves off the axis and there are concave regions around the poles, Fig. 4(c). This family of *inflected spheroids* limits to a *pinched spheroid*, Fig. 4(d), which is tangentially immersed on the axis and bounds a solid three-dimensional torus. Next, there are *immersed spheroids*, Fig. 4(e). Again, taking a limit, we obtain two surfaces asymptotic to a cylinder. One is an infinitely long prolate bubble (rotating liquid on the outside) which crosses the axis at one point and is asymptotic to the cylinder, Fig. 4(f). The other is a cylindro-antinodoid, which type we have already mentioned. The remaining *spheroids* correspond to bubbles and are concave and prolate, Fig. 4(g).

It should be emphasized that while the compact embedded examples have received much more attention in previous studies, portions of all of these surfaces are required to model rotating liquids in contact with a rotating container. Complete surfaces with self-intersections, of course, are non-physical when taken as a whole, but embedded portions of these same surfaces do correspond to physical interfaces. Fig. 5 indicates in cross-section how a binoid liquid interface might appear in an annular container.

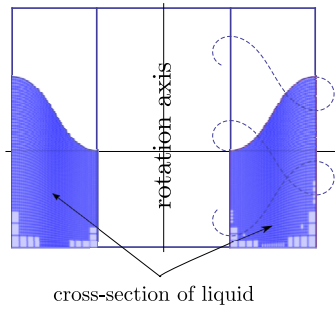


Fig. 5. Cross-section of a rotating annular container partially filled with liquid. The interface is modeled by a portion of a binoid.

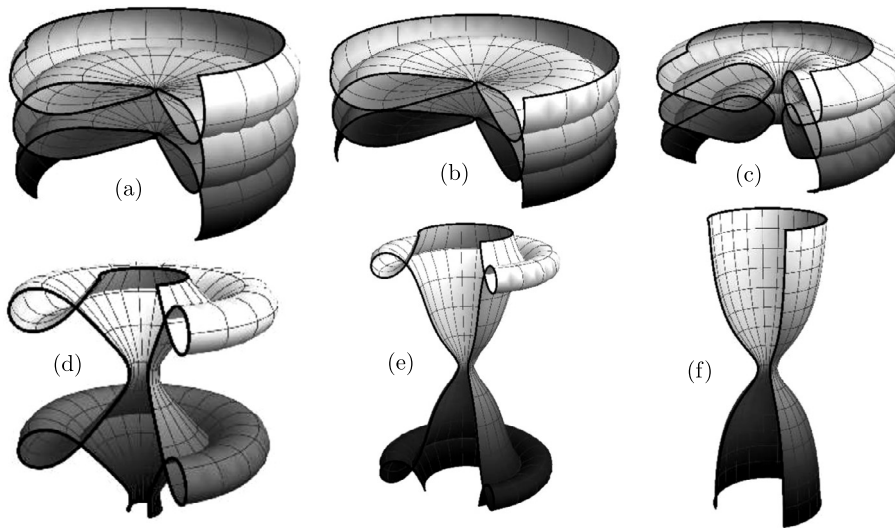


Fig. 6. (a) breaking nodoid (note the surface comes close to the axis but does not intersect it), (b) wobbleoid (inflections are not obvious in the graphic but are present), (c) breaking nodoid with higher degree of immersion, (d) breaking antinodoid, (e) antiwobbleoid (inflections are fairly obvious here), (f) cylindro-unduloid.

There is an additional family of distinct *nodoid type* surfaces. These may be distinguished from the ones mentioned above by the fact that the rotating liquids they model are considered to be on the opposite sides. These model the liquid inside the loops while the others model liquids outside the loops. In this family, additional deformations are possible.

One encounters here the appearance of an isolated inflection on the meridian. We call the corresponding surfaces *breaking nodoids*<sup>1</sup> as shown in Fig. 6(a) and (c). The deformation continues into surfaces whose meridians have the topology of a nodoid, but lose the key feature of being inflectionless. They have two changes of concavity within each half period. These we term *wobbleoids* or *inflected nodoids*, Fig. 6(b). These may be deformed so that the degree of immersion increases as described above with the nonconcavity being preserved to obtain inflected tori in the limit. The family of nodoid type surfaces with liquid inside the loops also limits to Gulliver’s tori of convex cross section.

In each case, the deformation may be continued through the toroidal solutions. Passing through Gulliver’s tori, one obtains antinodoids. Again, these are distinct from the antinodoids mentioned previously by virtue of a change of orientation of the mean curvature. In addition, these antinodoids admit deformation into *breaking* and *inflected antinodoids* (or *antiwobbleoids*) which are topologically like an antinodoid but have

<sup>1</sup> Our use of the term “breaking” here has a different meaning than it did for unduloid type surfaces, where it indicated a horizontal tangent at an inflection on the meridian. For nodoid type surfaces “breaking” simply indicates the appearance of an inflection on the meridian.

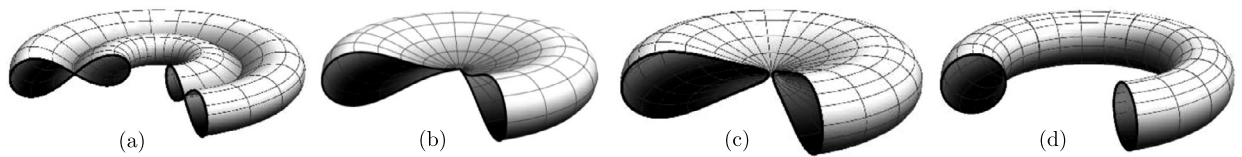


**Fig. 7.** (a) Immersed toroid (achtoid), (b) pinched spheroid (intersects the axis and may also be considered a spheroid), (c) nonconvex toroid, i.e., embedded toroid with nonconvex cross-section (note this surface comes very close to the axis but does not intersect it), (d) Gulliver toroid (convex cross-section). Between the family of nonconvex toroids and the Gulliver toroids, one finds the breaking toroids (not shown) which have convex cross-section and a pair of inflections on the meridian.

one or two inflections per half period respectively. A breaking antinodoid is shown in Fig. 6(d) and an antiwobbleid is shown in Fig. 6(e). These surfaces may also be deformed into inflected tori.

It is also possible to have unduloid type surfaces with the liquid to the outside. These are qualitatively the same as the unduloid type surfaces discussed above, though they are analytically different and admit a new kind of deformation leading to the last distinct qualitative type. Namely, it is possible to increase the period of these surfaces in such a way that a single inner neck is preserved and the limit surface is asymptotic to a cylinder, Fig. 6(f). Such a surface will be called a *cylindro-unduloid* and is always contained within the cylinder to which it is tangent, having a unique point of minimum radius and exactly two inflections. It is not possible to preserve a single bulge of an unduloid type surface. Aside from the tori, the basic deformations we have described are indicated in Fig. 6.

Four of the five qualitatively different toroids are indicated in Fig. 7. Technically, the pinched spheroid is a topological sphere tamely immersed at the poles and bounding a solid topological torus.

**The master list:** These are the names of the twenty-six qualitative types of rotational figures of equilibrium: cylinder, unduloid type, breaking unduloid, puzzle type, immersed puzzle type, immersed toroid (achtoid), binoid, cylindro-nodoid, cylindro-antinodoid, nodoid type, antinodoid, oblate spheroid, flat poled spheroid, inflected spheroid, pinched spheroid, immersed spheroid, infinite bubble, prolate spheroid, breaking nodoid, wobbleid/inflected nodoid, Gulliver toroid (convex cross-section), breaking toroid, nonconvex embedded toroid, breaking antinodoid, antiwobbleid/inflected antinodoid, cylindro-unduloid.

We now proceed to explain how these surfaces arise analytically in terms of physical parameters and prove various analytic and geometric properties of the deformations described heuristically above. The organization of the paper is as follows: In section 2, we classify rotational spheroids and unbounded figures of equilibrium. In section 3, we refine our classification techniques by considering “terminal heights” and characterize all rotational tori of equilibrium. We would like to thank Sarah McCuan for her help with making the illustrations.

## 2. Initial classification

### 2.1. Energy of a rotating drop

If a volume  $\mathcal{V}$  of liquid rigidly rotates, as described in the introduction, then we may take a frame of reference that rotates with the drop. With respect to this frame, the drop will be in apparent equilibrium. We assume the equilibrium shape minimizes an energy consisting of free surface energy and the potential energy associated with the centrifugal field  $\omega^2 \mathbf{r}$ . Explicitly we obtain

$$E = \sigma|\mathcal{S}| - \frac{1}{2}\rho\omega^2 \int_{\mathcal{V}} r^2, \quad (1)$$

where  $\sigma$  is a material dependent *surface tension*,  $\mathcal{S}$  is the boundary of  $\mathcal{V}$  or the *free surface*,  $\rho$  is the density of the drop,  $\omega$  is the angular velocity of rotation, and  $r$  is the distance to the axis of rotation. The expression (1) is determined only up to an additive constant.

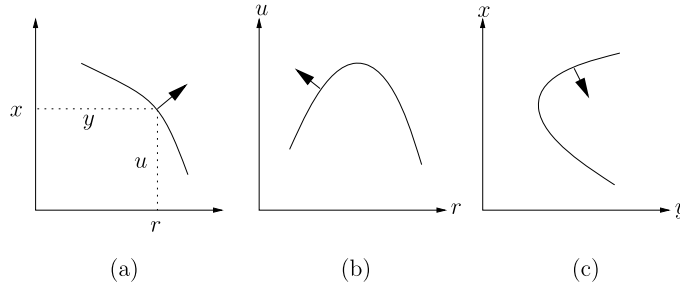


**Fig. 8.** Meridian curves and orientation.

Note that  $\rho$  is *not* the difference in densities of the two fluids, but we are assuming the outer fluid is not rotating, n.b., the assumption that the outer fluid is perfectly inviscid. Thus, in our chosen rotating frame the fluid exterior to the drop contributes centrifugal/potential energy to the system but also appears to rotate—adding kinetic energy of equal magnitude but opposite sign.

Under our assumptions, the observed interface provides a critical point for  $E$  with respect to *volume preserving variations*. It is well known that this is equivalent to providing a critical point for a modified energy

$$E_\ell = \sigma|\mathcal{S}| - \frac{1}{2}\rho\omega^2 \int_{\mathcal{V}} r^2 + 2\sigma\ell|\mathcal{V}| \tag{2}$$

where  $\ell$  is an appropriately chosen constant. Determining how  $\ell$  must be chosen in terms of the physical parameters, and the volume of  $\mathcal{V}$  in particular, is difficult—but important for experimental investigations. We do not address this question directly here but consider all possible axially symmetric critical surfaces for variational problems associated with energies of the form (2).

*2.1.1. Two coordinate expressions for E*

Every portion  $\mathcal{N}$  of a smooth meridian curve generating a critical surface for (2) may be locally expressed as either a function  $u = u(r)$  of radial distance  $r$  from the axis or as a function  $y = y(x)$  of height  $x$  along the axis. See Fig. 8(a). The corresponding energy expressions, up to the positive multiplicative constant  $2\pi\sigma$  and additive terms independent of the interior of  $\mathcal{N}$ , are given by

$$E_r(u) = \int \left( r\sqrt{1 + u'^2} - 4ar^3u + 2\ell ru \right) dr \tag{3}$$

and

$$E_h(y) = \int \left( y\sqrt{1 + y'^2} - ay^4 + \ell y^2 \right) dx \tag{4}$$

where  $a = \rho\omega^2/(8\sigma)$ .

These integrals should not be interpreted as indefinite, but are taken over the interval obtained by projecting  $\mathcal{N}$  onto the axis of the respective independent variable. Furthermore, while these integrals do not represent the total energy of the system, a variation of  $\mathcal{N}$  will result in the same change in one of these integrals (if it is well defined) as in the total energy.

*2.1.2. Euler–Lagrange equations*

The Euler–Lagrange equations associated to (3) and (4) are

$$\left( \frac{ru'}{\sqrt{1 + u'^2}} \right)' + 4ar^3 - 2\ell r = 0 \tag{5}$$

and

$$\left(\frac{yy'}{\sqrt{1+y'^2}}\right)' - \sqrt{1+y'^2} + 4ay^3 - 2\ell y = 0. \quad (6)$$

Each of these equations expresses the fact that the mean curvature  $H$  of the interface is a quadratic function of distance to the axis. In each case, the mean curvature is measured with respect to the “upward” normal; see Fig. 8(b), where the upward normal in  $(r, u)$  coordinates is shown, and Fig. 8(c), where the upward normal in  $(x, y)$  coordinates is shown. In either case the mean curvature is given by

$$2H = -4ar^2 + 2\ell. \quad (7)$$

The equation for the reflection of a solution across the  $r$  axis is obtained by switching the signs of both  $a$  and  $\ell$  in equation (5) or leaving them unchanged in equation (6).

## 2.2. Graphs over the radius; $u = u(r)$

We may integrate (5) to obtain

$$\frac{u'(r)}{\sqrt{1+u'(r)^2}} = -ar^3 + \ell r + \frac{c}{r} \quad (8)$$

where  $c$  is a constant of integration. Solutions of (8) depend, up to a vertical translation, on three parameters  $(a, \ell, c)$ . For nontrivial rotation, the parameter  $a$  may be eliminated by scaling. Indeed, if  $u = u(r)$  is a solution of (8) corresponding to parameters  $(a, \ell, c)$ , then

$$r \mapsto \sqrt[3]{a}u \left( \frac{r}{\sqrt[3]{a}} \right) \quad (9)$$

satisfies the same equation with parameters  $(1, \ell/\sqrt[3]{a}, \sqrt[3]{ac})$ . Thus up to a dilation of space, we may set  $a = 1$  and consider solutions of (8) depending on two parameters  $(\ell, c)$ .

Setting  $a = 1$  and

$$v(r) = -r^3 + \ell r + \frac{c}{r},$$

the equation (8) becomes simply

$$\sin \psi = v, \quad (10)$$

where  $\psi$  is the inclination angle the curve  $r \mapsto (r, u(r))$  makes with the positive  $r$ -axis. It follows that the meridians of rotational figures of equilibrium correspond to parameter values  $(\ell, c)$  for which

$$\{r > 0 : -1 \leq v(r) \leq 1\} \neq \emptyset. \quad (11)$$

Moreover, qualitative properties of such a meridian can be deduced directly from (10) or, equivalently, from the intersection of the graph of  $v = v(r)$  with the horizontal strip  $\Sigma = \{(r, t) : -1 \leq t \leq 1\}$ .

Fig. 9(a) indicates the relations between three plots of  $v(r)$  and the strip  $\Sigma$ . The first curve, determined by the pair  $(\ell, c) = (0, -3\sqrt[3]{2}/8 - 1/5)$ , does not intersect the strip and, thus, does not correspond to a solution. The second curve, determined by the pair  $(\ell, c) = (0, -3\sqrt[3]{2}/8)$ , is tangent to the strip and corresponds to a

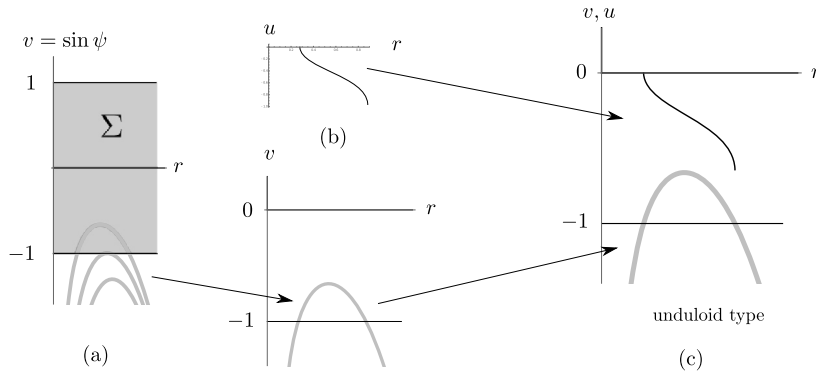


**Fig. 9.** On the left (a) we have shaded the strip  $\Sigma$  and indicated three plots of  $v$  for various values of  $\ell$  and  $c$ . The lowest curve does not intersect the strip and therefore does not correspond to a rotational figure of equilibrium. The next curve is tangent to the strip determining a unique radius for a circular cylindrical solution with negative mean curvature, i.e., liquid on the inside, which is a rotational figure of equilibrium for a particular collection of physical parameters. The last curve intersects the strip determining an interval  $(r_1, R)$  along the radial axis. In the middle (b), we have taken this meridian curve and plotted the corresponding solution  $u = u(r)$  for  $r_1 \leq r \leq R$  above it. Finally, on the right (c) we have combined the plots of  $v$  and  $u$ ; the vertical axis, in this case, represents different values for the plot of  $v$  (in thick gray) and the plot of  $u$  (in black). This particular meridian solution is of unduloid type, sharing the qualitative properties of a Delaunay unduloid. In the classification of solutions given below, the  $(\ell, c)$  parameter space is divided into three “quadrants” in rough analogy with the standard coordinate quadrants of a plane, but determined by changes in qualitative properties of solutions. The cylindrical surface is among the cylinders along the curve IIIa in Fig. 13. The unduloid type surface is in region IIIA of Fig. 13.

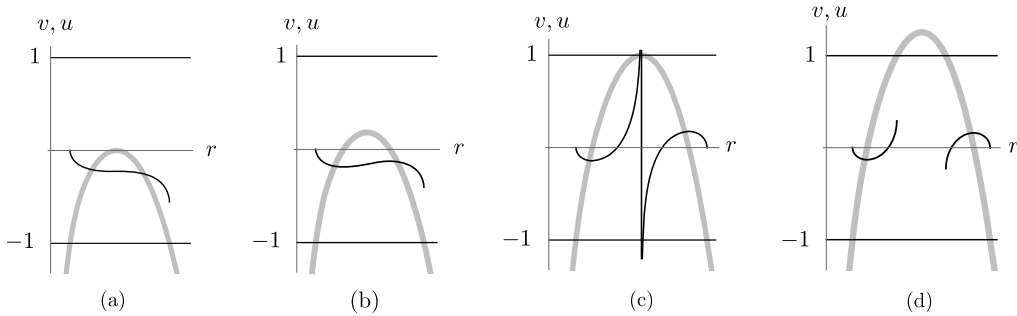


**Fig. 10.** (a) breaking unduloid ( $\ell = 2\sqrt{-c}$ ), (b) puzzle unduloid ( $2\sqrt{-c} < \ell < \ell_1(c)$ ), (c) cylindro-nodoid, cylinder, and cylindro-antinodoid ( $\ell = \ell_1(c)$ ) (d) nodoid-type and antinodoid ( $\ell_1(c) < \ell$ ). Here again, we have plotted  $v = \sin \psi$  in thick gray and a portion of the solution profile  $u = u(r)$  in black. The transition values  $\ell = \ell_1(c)$  and  $\ell = 2\sqrt{-c}$  for the parameter  $\ell$  are discussed below. In particular, the value  $\ell = \ell_1(c)$  is defined in Proposition 2.1.

circular cylinder of radius  $r = \sqrt[3]{2}/2$  according to Lemma 2.1 and Proposition 2.1 below. The third curve, determined by the pair  $(0, -3\sqrt[3]{2}/8 + 1/5)$ , corresponds to a solution  $u = u(r)$  as indicated in Fig. 9(b).

Notice the initial inclination of the meridian is  $\psi = -\pi/2$  when the radial value is a minimum  $r_1$ ; the inclination increases to a negative maximum (an inflection on the meridian) and then decreases back to  $\psi = -\pi/2$  at a maximum radial value  $R$ . It will be shown that this meridian extends periodically and shares the qualitative features of a Delaunay unduloid as indicated in Theorem 2.1 below.

In order to represent the various meridian types compactly and indicate certain qualitative properties, we have found it convenient to plot the graphs of  $v = v(r)$  and  $u = u(r)$  on the same axes as indicated in Fig. 9(c). It should be noted that the vertical axis in this case is playing a dual role, and the same scales are not always used for the two graphs. These observations provide a means for an initial classification of surfaces. Representative cases of the information encoded in these combined inclination/solution graphs are also indicated in Fig. 10.

We consider first the case of right circular cylinders. The following result follows directly from substitution in equation (7).

**Lemma 2.1.** *Assume  $(\ell, c) \in \mathbb{R}^2$  and there is some  $r_1 > 0$  such that*

$$|v(r_1)| = 1 \quad \text{and} \quad v'(r_1) = 0.$$

*Then associated to the parameter point  $(\ell, c)$  is a (solution) cylinder with radius  $r_1$ .*

For typical parameter points  $(\ell, c)$  corresponding to solution surfaces, the preimage in (11) contains an interval for which  $|v| = 1$  at the endpoints. The following result characterizes these surfaces.

**Theorem 2.1.** *Assume  $(\ell, c) \in \mathbb{R}^2$  and there are  $r_1, R > 0$  such that  $v(r) \in (-1, 1)$  for  $r \in (r_1, R)$  with  $|v(r_1)| = |v(R)| = 1$ . If*

$$v'(r_1) \neq 0 \quad \text{and} \quad v'(R) \neq 0, \tag{12}$$

*then associated to  $(\ell, c)$  is a smooth complete surface of revolution with meridian*

$$\cup_{k \in \mathbb{Z}} [\{(r, u(r) + 2hk) : r_1 \leq r \leq R\} \cup \{(r, -u(r) + 2hk) : r_1 \leq r \leq R\}]. \tag{13}$$

*The function  $u$  is given by*

$$u(r) = \int_{r_1}^r \frac{v(t)}{\sqrt{1 - v(t)^2}} dt, \quad r_1 \leq r \leq R \tag{14}$$

*and  $h = u(R)$ .*

**Proof.** The function  $u$  is finite valued and continuous as  $v$  has simple roots at  $r_1$  and  $R$ . It follows that the set defined in (13) is a continuous curve. We will verify that this curve is in fact smooth. Since  $u \in C^\infty(r_1, R)$  and the curve is periodic by construction, we need only check the points  $(r_1, 0)$  and  $(R, h)$ . The argument in each case is similar: Let us assume, without loss of generality, that  $v(r_1) = 1$ . In view of (14),  $u' > 0$  on an interval  $(r_1, r_1 + \delta]$  for  $\delta > 0$  chosen sufficiently small. Consequently,  $u$  restricted to  $[r_1, r_1 + \delta]$  has an inverse  $y_+ : [0, \epsilon] \rightarrow [r_1, r_1 + \delta]$  for some  $\epsilon > 0$ . Note that  $y_+(0) = r_1$ ,  $y'_+(0) = 0$  and  $y_+$  satisfies (6), that is,

$$\frac{y''(x)}{(1 + y'(x)^2)^{3/2}} - \frac{1}{y(x)\sqrt{1 + y'(x)^2}} = -4y(x)^2 + 2\ell \tag{15}$$

on  $(0, \epsilon)$ . On the other hand, the function  $y_-(x) := y_+(-x)$  defined for  $x \in [-\epsilon, 0]$  satisfies  $y_-(0) = r_1$ ,  $y'_-(0) = 0$  and satisfies (15) on  $(-\epsilon, 0)$ . Moreover,  $y_-$  is the inverse of  $-u$  restricted to  $[r_1, r_1 + \delta]$ .

Substituting  $y = y_+$  in (15) and sending  $x \rightarrow 0^+$  gives

$$y''_+(0+) - \frac{1}{r_1} = -4r_1^2 + 2\ell.$$

Likewise, if we substitute  $y = y_-$  in (15) and send  $x \rightarrow 0^-$ , we get

$$y''_-(0+) - \frac{1}{r_1} = -4r_1^2 + 2\ell.$$

Therefore, the function

$$y(x) := \begin{cases} y_-(x), & -\epsilon \leq x \leq 0 \\ y_+(x), & 0 \leq x \leq \epsilon \end{cases}$$

is  $C^2$  on  $(-\epsilon, \epsilon)$  and solves the ODE (15). As a result,  $y$  is smooth in some neighborhood of 0 which proves the claim.  $\square$

The surfaces described in the above theorem are *periodic* with half period

$$h = \int_{r_1}^R \frac{v(t)}{\sqrt{1 - v(t)^2}} dt.$$

Observe that  $h$  is a function of the parameters  $(\ell, c)$ . A detailed discussion of  $h$  is given in the following section. Values  $(\ell, c)$  for which  $h$  vanishes are of particular note; these correspond to rotational tori of equilibrium.

The next class of surfaces we consider occur when one of the conditions in (12) fails. In this case, the associated parameters correspond to solutions that are asymptotic to cylinders (in addition to the cylinders described in Lemma 2.1).

**Theorem 2.2.** *Assume  $(\ell, c) \in \mathbb{R}^2$  and that there are  $r_1, R > 0$  such that  $v(r) \in (-1, 1)$  for  $r \in (r_1, R)$  with  $|v(r_1)| = |v(R)| = 1$ . If*

$$v'(r_1) \neq 0 \quad \text{and} \quad v'(R) = 0,$$

*then associated to  $(\ell, c)$  is a smooth complete surface of revolution with profile*

$$\{(r, u(r)) : r_1 \leq r < R\} \cup \{(r, -u(r)) : r_1 \leq r < R\}. \tag{16}$$

*The function  $u$  is given by*

$$u(r) = \int_{r_1}^r \frac{v(t)}{\sqrt{1 - v(t)^2}} dt, \quad r_1 \leq r < R.$$

*This surface of revolution is asymptotic to a cylinder with radius  $R$ .*

**Remark 2.1.** *A similar conclusion follows if we assume  $v'(r_1) = 0$  and  $v'(R) \neq 0$ .*

**Proof.** We can argue as in the previous assertion to verify that the curve (16) corresponds to a smooth meridian curve. Therefore, we focus on verifying  $u(r)$  tends to infinity as  $r$  tends to  $R$  from below. Again, we may assume  $v(R) = 1$  as the alternative case is similar.

Choose  $\epsilon > 0$  sufficiently small, so that  $v \in [1/2, 1]$  on  $[R - \epsilon, R]$ . Note for  $r \in [R - \epsilon, R]$

$$\begin{aligned} \int_{R-\epsilon}^r \frac{v(t)}{\sqrt{1 - v(t)^2}} dt &= \int_{R-\epsilon}^r \frac{v(t)}{\sqrt{1 + v(t)}} \frac{1}{\sqrt{1 - v(t)}} dt \\ &\geq \int_{R-\epsilon}^r \frac{1/2}{\sqrt{2}} \frac{1}{\sqrt{1 - v(t)}} dt \\ &= \frac{1}{2\sqrt{2}} \int_{R-\epsilon}^r \frac{1}{\sqrt{1 - v(t)}} dt. \end{aligned} \tag{17}$$

Expanding  $1 - v$  in a Taylor series about  $R$ , we get

$$1 - v(r) = -\frac{1}{2}v''(R)(r - R)^2 + o(r - R)^2 \tag{18}$$

as  $r \rightarrow R$ .

Since  $v < 1$  on  $(r_1, R)$ , (18) implies  $v''(R) \leq 0$ . In particular, for  $\epsilon$  chosen small enough

$$1 - v(r) \leq \left(-\frac{1}{2}v''(R) + 1\right)(R - r)^2, \quad R - \epsilon \leq r < R.$$

Combining this inequality with (17) gives

$$\begin{aligned} \int_{R-\epsilon}^r \frac{v(t)}{\sqrt{1-v(t)^2}} dt &\geq \frac{1}{2\sqrt{(2-v''(R))}} \int_{R-\epsilon}^r \frac{1}{R-t} dt \\ &= \frac{1}{2\sqrt{(2-v''(R))}} \ln\left(\frac{\epsilon}{R-r}\right) \end{aligned}$$

for  $r \in [R - \epsilon, R)$ . Thus,

$$\lim_{r \rightarrow R^-} \int_{R-\epsilon}^r \frac{v(t)}{\sqrt{1-v(t)^2}} dt = +\infty.$$

As a result,  $\lim_{r \rightarrow R^-} u(r) = +\infty$ .  $\square$

The only surfaces to which the general results above do not apply directly arise when  $c = 0$ . In this case  $v$  is a cubic polynomial that always has a root at  $r = 0$ . When we have additionally that  $\ell < 3/\sqrt[3]{4}$ , then  $|v(R)| = 1$  always has a unique positive root  $R$ ; one finds  $v(R) = -1$  and  $v'(R) < 0$ , so there is a unique solution which models a compact rotating drop (liquid inside). This one parameter family of rotational figures of equilibrium includes the family of spheroids studied by Rayleigh, Beer, and Chandrasekhar. See Fig. 11. When  $\ell \geq 3/\sqrt[3]{4}$ , the equation  $|v(R)| = 1$  has multiple solutions; some of these solutions satisfy  $v(R) = 1$  and correspond to bubbles (liquid outside). The arguments we have presented above, with minor modifications, yield the following result.

**Corollary 2.1.** *Assume  $c = 0$ ,  $\ell \in \mathbb{R}$ , and that there is some  $R > 0$  such that  $v(r) \in (-1, 1)$  for  $r \in [0, R)$  with  $|v(R)| = 1$ . If  $v'(R) \neq 0$ , then associated to  $\ell$  is a smooth compact surface of revolution with profile*

$$\{(r, u(r) - u(R)) : 0 \leq r \leq R\} \cup \{(r, -u(r) + u(R)) : 0 \leq r \leq R\}.$$

The function  $u$  is given by

$$u(r) = \int_0^r \frac{v(t)}{\sqrt{1-v(t)^2}} dt, \quad 0 \leq r \leq R.$$

Alternatively, if  $v'(R) = 0$ , then associated to  $\ell$  is a smooth complete surface of revolution with profile

$$\{(r, u(r)) : 0 \leq r < R\}$$

In this case, the integral representation given above holds for  $0 \leq r < R$  with  $\lim_{r \nearrow R} u(r) = +\infty$  and the surface is asymptotic to a cylinder from within. See, for example, Fig. 4(f).

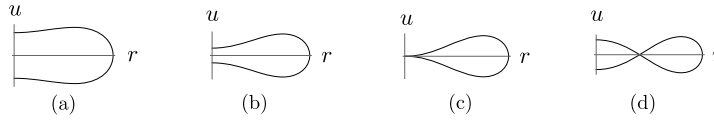


**Fig. 11.** The process of pinching spheroids. In this case  $c = 0$ ;  $0 < \ell < 3/\sqrt[3]{4}$ . (a–c) indicate physical embedded drops for increasing  $\ell$  while (d) has become immersed.

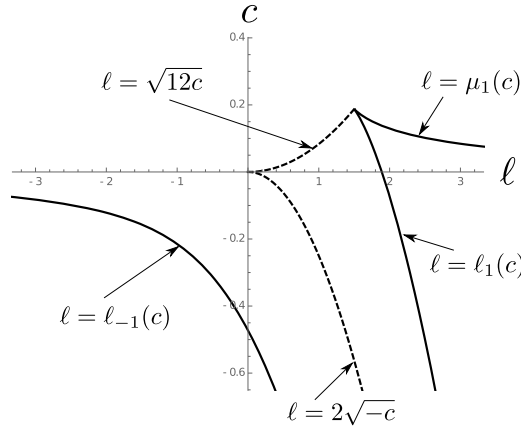


**Fig. 12.** Transition curves in  $(\ell, c)$  parameter space. The curve  $\ell = \ell_{-1}(c)$  is a curve representing cylinders (liquid inside) and the only non-existence curve; there are no surfaces corresponding to  $\ell < \ell_{-1}$ . In addition,  $\ell = \ell_{-1}(c)$  is also a boundary of unduloid type solutions (liquid inside). The curve  $\ell = 2\sqrt{-c}$  represents breaking of the profile in these “unduloid” type solutions in which the meridians cease to be graphs. The curve  $\ell = \ell_1(c)$  denotes a limiting transition associated with the appearance of cylinders (liquid outside) accompanied by various other solutions depending particularly on the sign of  $c$ . The curve  $\ell = \sqrt{12c}$  separates meridians of “nodoid” type with no inflections ( $0 < c < 3/16$  and  $\ell < \sqrt{12c}$ ) from those with two inflections per half period. The solutions for  $0 < c < 3/16$  and  $\ell = \sqrt{12c}$  have a single inflection per half period, but no change of concavity, and are termed *breaking* nodoid (or antinodoid) type. Finally, the curve  $\ell = \mu_1(c)$  denotes another appearance of cylinders (liquid outside) and the extinction of a second unduloid type family (liquid outside). See also Fig. 13 below.

Using the results above along with a straightforward analysis of the rational function  $v = v(r)$ , one finds the initial collection of curves, indicated in Fig. 12. These curves generally correspond to qualitative changes of solutions. There is a secondary collection of curves, associated primarily with changes in the degree of immersion. The most important of these is the torus curve  $h = 0$  indicated in Fig. 17. It is possible, as discussed briefly below, to determine the precise degree of immersion for solutions near the solid curves of Fig. 12 and Fig. 13. These curves represent the parameter points  $(\ell, c)$  for which the equation  $|v(r)| = 1$  has a root of multiplicity two and, thus, where cylinders occur. The *cylinder curves* are determined explicitly and we now summarize their properties.

**Proposition 2.1.** *Let  $(\ell, c) \in \mathbb{R}^2$ . The equations*

$$|v(r)| = 1, \quad v'(r) = 0$$

*have a positive solution  $r$  if and only if one of the following hold:*

- (i)  $c < 0$  and

$$\ell = \ell_{-1}(c) := 3t^2 + \frac{c}{t^2},$$

*where  $t$  is the unique positive solution of  $2t^4 + t + 2c = 0$ ;*

- (ii)  $c \leq 3/16$  and

$$\ell = \ell_1(c) := 3t^2 + \frac{c}{t^2},$$

*where  $t$  is the largest positive solution of  $2t^4 - t + 2c = 0$ ;*

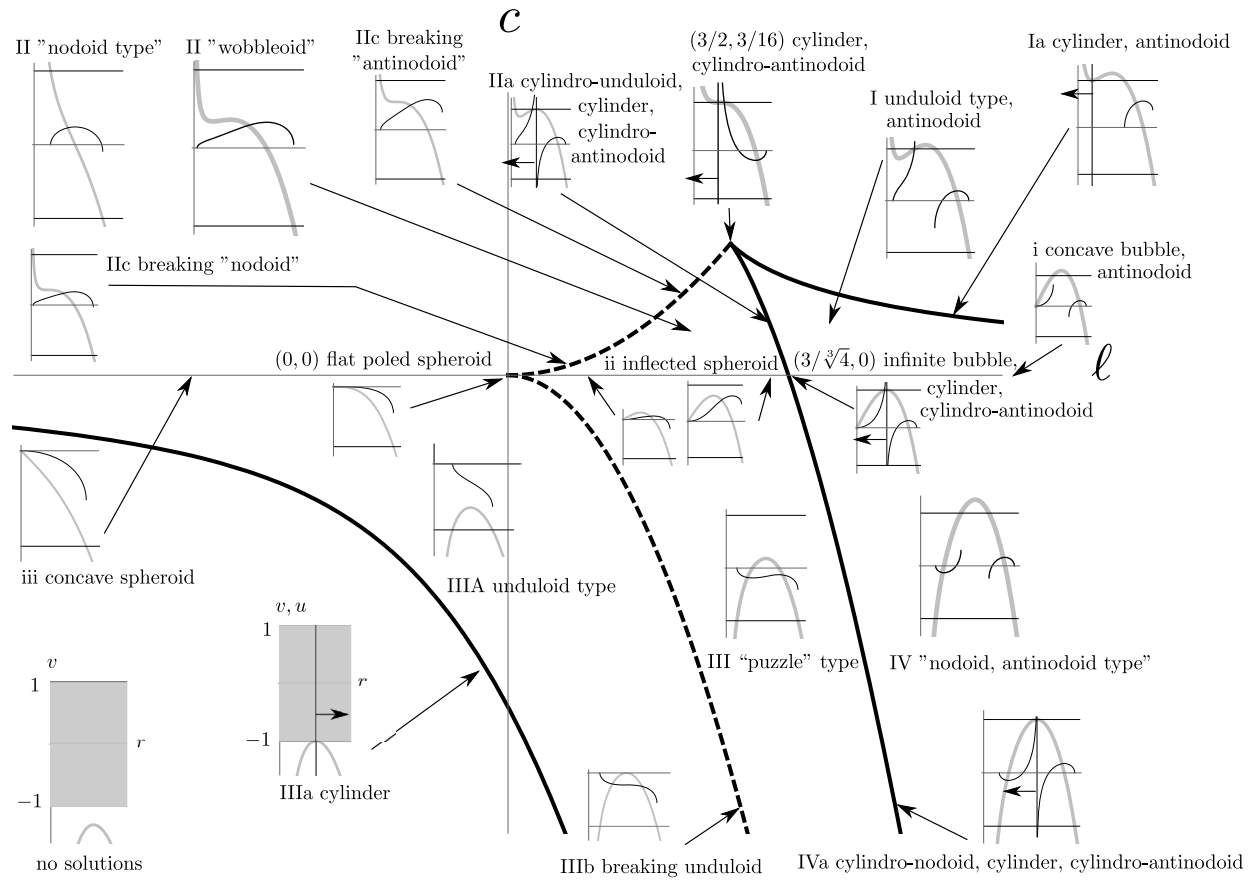


**Fig. 13.** First pass through parameter space. In this illustration we have inset plots of  $v = \sin \psi$  and  $u = u(r)$  in the  $(\ell, c)$  parameter space to illustrate various solutions. The axes of the insets are not labeled except for the two in the lower left corner in which the strip  $\{(r, t) : -1 \leq t \leq 1\}$  is also shaded. The normal pointing out of the liquid is indicated for cylinders.

(iii)  $0 < c \leq 3/16$  and

$$\ell = \mu_1(c) := 3t^2 + \frac{c}{t^2},$$

where  $t$  is the smallest positive solution  $2t^4 - t + 2c = 0$ .

The first cylinder curve determined by  $\ell = \ell_{-1}(c)$  is concave and asymptotic to the negative  $\ell$ -axis. Each solution corresponds only to a cylinder, and there are no solutions for  $\ell < \ell_{-1}(c)$ . This is the only boundary for nonexistence in the  $(\ell, c)$  parameter plane.

Since we refer to an explicit value associated with the first cylinder curve, we record that expression here. For  $c < 0$ , the function  $v = v(r)$  is concave and attains a unique maximum at some  $r_{\max} = r_{\max}(\ell, c)$ . In fact,

$$r_{\max} = \sqrt{\frac{\ell + \sqrt{\ell^2 - 12c}}{6}} > 0. \tag{19}$$

The first cylinder curve  $\ell = \ell_{-1}$  may also be expressed as a level set  $\{(\ell, c) : v(r_{\max}) = -1\}$ .

The second cylinder curve has a corner at  $(\ell, c) = (3/2, 3/16)$  and is asymptotic to the positive  $\ell$ -axis. The portion determined by  $\ell = \ell_1(c)$  is concave while the portion  $\ell = \mu_1(c)$  is convex. Each point corresponds to a surface asymptotic to a cylinder.

Parameters not belonging to those curves correspond to surfaces that are either periodic (and possibly toroidal) or are in the spheroid family.

The two dashed curves in Fig. 12 follow from a similar elementary analysis. Their explicit expressions are even simpler:  $\ell = 2\sqrt{-c}$  for  $c < 0$  and  $\ell = \sqrt{12c}$  for  $0 < c < 3/16$ , which correspond to the appearance of critical points and inflections in the meridian respectively.

Fig. 13 represents visually the qualitative distinctions which are determined by our initial classification. We recall that a discussion of how to interpret the insets in this figure is given above. In Fig. 9(c) the function  $v$  is plotted in thick gray along with the corresponding meridian for  $(\ell, c)$  in a region adjoining the first cylinder curve. The sign of  $v$  matches the sign of  $u'$  and hence the monotonicity of the meridian given by  $u = u(r)$  is known: The solution  $u$  decreases from  $u(r_1) = 0$  to  $u(R) < 0$  with a single inflection corresponding to  $r = R$  as indicated. Theorem 2.1 applies, and the meridian is of unduloid type.

Some regions are left ambiguous as indicated by quotation marks because this initial classification does not provide some necessary information on the value of the half period  $h = u(R)$ . The relative height of an inflectionless loop (“nodoid type” or “antinodoid”) is known in all cases where  $v = v(r)$  is concave or convex on the interval of definition. This follows from the convexity-height lemma of [6], which we also state (Lemma 3.2) and refine in the next section. This eliminates the ambiguity of the quotation marks in the upper left region II (nodoid type) and the lower right region IV (nodoid and antinodoid type).

This initial classification, furthermore, determines precisely the qualitative type of all solutions on and in neighborhoods of the cylinder curves and on the dashed curve in the fourth quadrant.

As mentioned above, the toroid curve of Fig. 17 is not indicated in Fig. 13. Certain qualitative distinctions are also omitted from Fig. 13 due to space limitations. Of particular note are the following: The torus curve separates the portion IIc of the “breaking nodoid” curve into breaking nodoids (on the left) and breaking antinodoids (on the right). The antiwobbleoids (or inflected antinodoids) are not shown and are to the right of the torus curve in region II. The immersed spheroids correspond to a segment on the axis between the torus curve and the second cylinder curve; the left endpoint corresponds to the pinched spheroid. The binoids are not shown and are to the right of the torus curve in region III. Finally, there are five kinds of toroids which occur in obvious succession along the torus curve. The analysis of the torus curve itself is addressed in the following section.

### 3. Terminal heights

As described above, the terminal heights  $h = u(R)$  distinguish between nodoid type surfaces and antinodoid type surfaces with zero values corresponding to toroidal solutions. Given the continuity of the terminal height  $h$  with respect to  $\ell$  and  $c$ , one concludes, as in [6], that a transition involving toroidal solutions must take place along each parameter line  $c = \text{constant}$ . In the next section, we provide a proof of the required continuity and show the transition must take place in a well-defined, relatively narrow strip.

We begin with some preliminary results (including the fundamental continuity result) and auxiliary results of independent interest for the geometric dependence of surfaces (including unduloid type) on the parameters  $\ell$  and  $c$ .

#### 3.1. Continuity

Let  $r = r_1$  and  $R$  denote specified simple roots of polynomial equations with coefficients depending on the parameters  $\ell$  and  $c$  and corresponding to one qualitative type of solution in a region of the  $(\ell, c)$ -plane as described above. Then

$$h = \int_r^R \frac{v(t)}{\sqrt{1 - v(t)^2}} dt$$

represents the corresponding terminal height, and  $h = h(\ell, c)$  is a well-defined continuous function in that region of the  $(\ell, c)$ -plane. Though this assertion is often quoted (even in our own paper [6]), we are unaware of a detailed proof in the literature. We will need a somewhat more general version below, so we provide a proof here.

**Lemma 3.1.** *Let  $Q \subset \mathbb{R}^2$  be an open and bounded region. Let  $r$  and  $R$  denote positive continuous functions on  $Q$  satisfying  $r < R$ . If  $f : (0, \infty) \times Q \rightarrow \mathbb{R}$  is locally Lipschitz continuous and satisfies*

$$\sqrt{(t-r)(R-t)} f(t, q) \leq M \tag{20}$$

for  $q \in Q$ ,  $r(q) < t < R(q)$ , and some constant  $M$ , then

$$w(q) := \int_{r(q)}^{R(q)} f(t, q) dt$$

is continuous on  $Q$ .

**Proof.** Let  $\epsilon > 0$  and let  $q_0 \in Q$  be fixed. We first claim that for  $\delta > 0$  small enough,

$$\left| \int_{r(q)}^{r(q)+\delta} f(t, q) dt \right| < \frac{\epsilon}{8} \quad \text{for } |q - q_0| < \delta. \tag{21}$$

To see this, note first that for all  $\delta$  small enough, owing to the continuity of  $R - r$  at  $q_0$ , we will have

$$R(q) - r(q) - \delta > \frac{R(q_0) - r(q_0)}{2}.$$

It may also be assumed, without loss of generality, that we have in addition to (20)

$$M \geq \frac{1}{\sqrt{R(q) - r(q)}} \geq \frac{1}{2\sqrt{R(q_0) - r(q_0)}} \quad \text{for } |q - q_0| < \delta.$$

Then

$$\begin{aligned} \left| \int_{r(q)}^{r(q)+\delta} f(t, q) dt \right| &\leq \int_{r(q)}^{r(q)+\delta} \frac{M}{\sqrt{(t-r)(R-t)}} dt \\ &\leq \int_{r(q)}^{r(q)+\delta} \frac{4M^2}{\sqrt{t-r(q)}} dt \\ &= 8M^2\sqrt{\delta}. \end{aligned}$$

If we further require  $\sqrt{\delta} < \epsilon/(64M^2)$ , the claim is established. Similarly, for all  $\delta$  small enough, we will have

$$\left| \int_{R(q)-\delta}^{R(q)} f(t, q) dt \right| < \frac{\epsilon}{8} \quad \text{for } |q - q_0| < \delta. \tag{22}$$

In particular, we may take  $\delta_0 > 0$  small enough so that (21) and (22) hold for  $0 < \delta < \delta_0$ . Moreover, for  $0 < \delta < \delta_0$

$$\begin{aligned}
 |w(q) - w(q_0)| &= \left| \int_{r(q)}^{R(q)} f(t, q) dt - \int_{r(q_0)}^{R(q_0)} f(t, q_0) dt \right| \\
 &\leq \frac{\epsilon}{2} + \left| \int_{r(q)+\delta_0}^{R(q)-\delta_0} f(t, q) dt - \int_{r(q_0)+2\delta_0}^{R(q_0)-2\delta_0} f(t, q) dt \right|.
 \end{aligned}$$

When  $\delta$  is sufficiently small and  $|q - q_0| < \delta$ , we will also have

$$r(q) + \delta_0 < r(q_0) + 2\delta_0 < R(q_0) - 2\delta_0 < R(q) - \delta_0.$$

Thus,

$$\begin{aligned}
 |w(q) - w(q_0)| &\leq \frac{3\epsilon}{4} + \left| \int_{r(q_0)+2\delta_0}^{R(q_0)-2\delta_0} [f(t, q) - f(t, q_0)] dt \right| \\
 &\leq \frac{3\epsilon}{4} + \int_{r(q_0)+2\delta_0}^{R(q_0)-2\delta_0} |f(t, q) - f(t, q_0)| dt.
 \end{aligned}$$

Since

$$\{(t, q) : r(q_0) + 2\delta_0 < t < R(q_0) - 2\delta_0, |q - q_0| < \delta\}$$

is fixed and compactly contained in  $\mathcal{Q}$ , there is some  $\Lambda > 0$  so that

$$|f(t, q) - f(t, q_0)| \leq \Lambda|q - q_0| < \Lambda\delta.$$

Finally for  $|q - q_0| < \delta$  small enough

$$|w(q) - w(q_0)| < \frac{3\epsilon}{4} + (R(q_0) - r(q_0))\Lambda\delta < \epsilon. \quad \square$$

### 3.2. Limiting values

Having established the continuity of the terminal height as a function of the parameters  $\ell$  and  $c$ , we now consider the limiting values as the parameters approach the initial transition curves. We begin with unduloid type surfaces for parameters approaching the first cylinder curve. As a particular cylinder (liquid outside) is approached, a characteristic length for the period of the unduloid type surfaces may be extracted.

**Theorem 3.1.** *For  $c < 0$  and  $\ell_{-1}(c) < \ell < \ell_1(c)$ , the “unduloid” type solutions satisfy*

$$\lim_{\ell \searrow \ell_{-1}(c)} h(\ell, c) = -\pi \sqrt{\frac{r^3}{2(3r^4 - c)}},$$

where  $r$  is the unique positive root of the equation  $2r^4 + r + 2c = 0$ .

**Proof.** Let  $r_1$  denote the smallest solution of  $v(r) = -1$ . Let  $r_{\max}$  denote the value given in (19). Note that, in the limit under consideration, the values of  $r_1$ ,  $r_{\max}$ , and  $R$  all limit to a value  $r$  satisfying the quartic equation given in the statement of the theorem. For the unduloid type surfaces in question we have

$$\begin{aligned}
 h &= \int_{r_1}^{r_{\max}} \frac{v(t)}{\sqrt{1-v(t)^2}} dt + \int_{r_{\max}}^R \frac{v(t)}{\sqrt{1-v(t)^2}} dt \\
 &= (r_{\max} - r) \int_0^1 \frac{v(r_{\max} + (r_1 - r_{\max})\tau)}{\sqrt{1-v(r_{\max} + (r_1 - r_{\max})\tau)^2}} d\tau \\
 &\quad + (R - r_{\max}) \int_0^1 \frac{v(r_{\max} + (R - r_{\max})\tau)}{\sqrt{1-v(r_{\max} + (R - r_{\max})\tau)^2}} d\tau
 \end{aligned}$$

where we have used the change of variables  $\tau = (t - r_{\max})/(r_1 - r_{\max})$  in the first integral and  $\tau = (t - r_{\max})/(R - r_{\max})$  in the second.

Let us consider the first integral. A calculation shows

$$1 + v(r_{\max} + (r_1 - r_{\max})\tau) = (r_1 - r_{\max})^2(1 - \tau^2)f(r_1, r_{\max}, \tau)$$

where

$$\begin{aligned}
 f(r_1, r_{\max}, \tau) &= r_1 + 2r_{\max} - \frac{c}{r_1 r_{\max} (r_{\max} + (r_1 - r_{\max})\tau)} \\
 &\quad + \frac{r_1 - r_{\max}}{1 + \tau} \left( \tau^2 - \frac{c}{r_1 r_{\max}^2 (r_{\max} + (r_1 - r_{\max})\tau)} \right).
 \end{aligned}$$

Observe that  $f(r_1, r_{\max}, \tau)$  converges uniformly in  $\tau$  as  $\ell \searrow \ell_{-1}(c)$  to the constant

$$f(r, r, \tau) = 3r - \frac{c}{r^3} = -\frac{1}{2}v''(r)$$

where  $r = r(c)$  is the common limiting value given in the statement of the theorem. Thus, an elementary application of the dominated convergence theorem yields

$$\begin{aligned}
 \lim_{\ell \searrow \ell_{-1}(c)} \int_{r_1}^{r_{\max}} \frac{v(t)}{\sqrt{1-v(t)^2}} dt &= -\frac{1}{\sqrt{2f(r, r, \tau)}} \sin^{-1}(\tau) \Big|_{\tau=0}^1 \\
 &= -\frac{\pi}{2} \sqrt{\frac{r^3}{2(3r^4 - c)}}.
 \end{aligned}$$

Similar reasoning gives the same value for limit of the second integral.  $\square$

We next consider limits of the terminal heights for solutions corresponding to parameters approaching the second cylinder curve  $\ell = \ell_1(c)$  for  $c < 3/16$ .

**Theorem 3.2.** *For  $c < 0$  and  $\ell_{-1}(c) < \ell < \ell_1(c)$  “unduloid” type solutions satisfy*

$$\lim_{\ell \nearrow \ell_1(c)} h(\ell, c) = +\infty.$$

*For  $c < 0$  and  $\ell > \ell_1(c)$  “nodoid” and “antinodoid” type solutions satisfy*

$$\lim_{\ell \searrow \ell_1(c)} h(\ell, c) = +\infty.$$

For  $c = 0$  and  $\ell < \ell_1(0)$  “immersed drop” solutions satisfy

$$\lim_{\ell \nearrow \ell_1(0)} h(\ell, 0) = +\infty.$$

For  $c = 0$  and  $\ell < \ell_1(0)$  and  $\ell > \ell_1(0)$  “concave bubble” and “antinodoid” type solutions satisfy

$$\lim_{\ell \searrow \ell_1(0)} h(\ell, 0) = +\infty.$$

For  $0 < c < 3/16$  and  $\ell < \ell_1(c)$  “wobbleoid” solutions satisfy

$$\lim_{\ell \nearrow \ell_1(c)} h(\ell, c) = +\infty.$$

For  $0 < c < 3/16$  and  $\ell_1(c) < \ell < \mu_1(c)$  “unduloid” and “antinodoid” type solutions satisfy

$$\lim_{\ell \searrow \ell_1(c)} h(\ell, c) = +\infty.$$

In summary, this theorem asserts that for  $c < 3/16$  all terminal heights tend to positive infinity as  $\ell$  approaches  $\ell_1(c)$ . The result follows from the limiting arguments in [6] or from straightforward modifications of those arguments; we omit the details.

We next turn to the characteristic height associated with unduloid type solutions corresponding to parameters close to the other portion of the second cylinder curve.

**Theorem 3.3.** For  $0 < c < 3/16$  and  $\ell_1(c) < \ell < \mu_1(c)$  “unduloid” solutions satisfy

$$\lim_{\ell \nearrow \mu_1(c)} h(\ell, c) = \pi \sqrt{\frac{r^3}{2(c - 3r^4)}},$$

where  $r$  is the smaller positive root of the equation  $2r^4 - r + 2c = 0$ .

The proof is a straightforward modification of that given above for [Theorem 3.1](#).

Finally, we consider solutions corresponding to parameters with  $|\ell|$  tending to infinity.

**Theorem 3.4.** For  $c < 0$  and  $\ell > \ell_1(c)$  “nodoid” and “antinodoid” type solutions satisfy

$$\lim_{\ell \nearrow \infty} h(\ell, c) = 0.$$

For  $c = 0$  and  $\ell < \ell_1(0)$  “spheroid” type solutions satisfy

$$\lim_{\ell \searrow -\infty} h(\ell, 0) = 0.$$

For  $c = 0$  and  $\ell > \ell_1(0)$  “concave bubble” and “antinodoid” type solutions satisfy

$$\lim_{\ell \nearrow \infty} h(\ell, 0) = 0.$$

For  $c > 0$  “nodoid” type solutions satisfy

$$\lim_{\ell \searrow -\infty} h(\ell, c) = 0.$$

For  $c > 0$  “antinodoid” type solutions satisfy

$$\lim_{\ell \nearrow \infty} h(\ell, c) = 0.$$

In summary, as  $|\ell|$  tends to infinity all terminal heights tend to zero.

**Proof.** We give a proof for the “nodoid” type solutions with  $c < 0$  and  $\ell > \ell_1(c)$ . In this case, we have  $v = v(t)$  is concave with a unique zero at  $t = t_1$ . As above,

$$h = \int_{r_1}^R \frac{v(t)}{\sqrt{1-v(t)^2}} dt = \int_{r_1}^{t_1} \frac{v(t)}{\sqrt{1-v(t)^2}} dt + \int_{t_1}^R \frac{v(t)}{\sqrt{1-v(t)^2}} dt.$$

Moreover,

$$v(t) \leq 0, \quad r_1 \leq t \leq t_1$$

and

$$v(t) \leq 1 + v'(R)(t - R), \quad t_1 \leq t \leq R.$$

Consequently,

$$\int_{r_1}^{t_1} \frac{v(t)}{\sqrt{1-v(t)^2}} dt \leq 0$$

and

$$\int_{t_1}^R \frac{v(t)}{\sqrt{1-v(t)^2}} dt \leq \frac{\sqrt{1-(Rv'(R))^2}}{v'(R)} \leq \frac{1}{v'(R)}.$$

Thus,

$$0 \leq h(\ell, c) \leq \frac{1}{v'(R)}$$

where the left inequality follows from [Lemma 3.2](#) below.

Differentiating  $v(R) = 1$  with respect to  $\ell$  gives

$$\frac{\partial R}{\partial \ell} = -\frac{R}{v'(R)} < 0.$$

Since  $R > 0$ , the limit of  $R$  as  $\ell \rightarrow \infty$  exists and is nonnegative. By rewriting  $v(R) = 1$  as

$$-\frac{R^4}{\ell} + R^2 + \frac{c}{\ell} = \frac{R}{\ell},$$

we may easily conclude  $R \rightarrow 0$  as  $\ell \rightarrow \infty$ . As  $v'(R) = -3R^2 + \ell - c/R^2 \rightarrow +\infty$ , as  $\ell \rightarrow \infty$ , we also have

$$\lim_{\ell \rightarrow \infty} h(\ell, c) = 0. \quad \square$$

### 3.3. Preliminary torus estimates

Lemma 3.1 was used along with results on the sign of  $h$  in [6] to show the existence of at least one toroidal solution for each  $c \in \mathbb{R}$ . The main tool used in that paper to obtain results on the sign of  $h$  was the following:

**Lemma 3.2** (*General convexity-height lemma for rotational surfaces*). Assume  $0 < r < R$  and  $v : [r, R] \rightarrow [-1, 1]$  is continuous and decreasing with  $v(r) = 1$  and  $v(R) = -1$ . If  $v$  is convex, then

$$h = \int_r^R \frac{v}{\sqrt{1-v^2}} dr < 0.$$

Similarly, if  $v$  is concave, then  $h > 0$ .

One simple application of the convexity-height lemma is the following: Each point in the region

$$A = \{(\ell, c) : \ell_1(c) < \ell < \mu_1(c), 0 < c < 3/16\} \tag{23}$$

corresponds to two solutions. One of these is known to be of unduloid type with  $v = \sin \psi > 0$ . The other has  $v = \sin \psi$  concave so that the convexity-height lemma applies, we know  $h > 0$ , and the solution is of anti-nodoid type.

It also follows from the convexity-height lemma that each solution corresponding to  $c > 0$  and

$$\ell \leq -2\sqrt{\frac{c}{3}} - \sqrt[4]{\frac{3}{c}}$$

is of nodoid type ( $h < 0$ ), and any non-cylindrical solution corresponding to  $c > 0$  and

$$\ell \geq \max \left\{ -2\sqrt{\frac{c}{3}} + \sqrt[4]{\frac{3}{c}}, \mu_1(c) \right\}$$

is of anti-nodoid type ( $h > 0$ ). Our convention is that the maximum above is equal to  $-2\sqrt{c/3} + \sqrt[4]{3/c}$  when  $\mu_1(c)$  is not defined. We now wish to sharpen this result.

**Lemma 3.3.** *If  $c > 0$  and  $\ell \leq -2\sqrt{c/3}$ , then  $h < 0$  and the corresponding surface is of nodoid type.*

**Proof.** Following the first part of the proof of the convexity-height lemma from [6], we let  $t_0$  denote the unique root of  $v(t) = \sin \psi(t) = 0$  and use the change of variables

$$v(\tau) = -v(t) \tag{24}$$

on the interval  $[t_0, R]$ . We thus obtain

$$h = \int_r^{t_0} \left( 1 - \frac{v'(t)}{v'(\tau)} \right) \frac{v(t)}{\sqrt{1-v(t)^2}} dt$$

where  $\tau = \tau(t)$  is defined implicitly by (24).

Since  $u' = v/\sqrt{1-v^2} > 0$  on  $(r, t_0)$ , it is enough to show

$$v'(t) < v'(\tau) < 0 \quad \text{for } r < t < t_0. \quad (25)$$

Equivalently, we wish to show

$$f(t, \ell) = v'(\tau) - v'(t)$$

is nonnegative for  $r \leq t \leq t_0$  with strict inequality at some point. In fact, we will show this quantity is strictly positive unless  $\ell = -2\sqrt{c/3}$  and  $t = t_0$ .

There is also a unique positive root of  $v''(t) = 0$  which we denote by  $t_1$ . The conditions  $c > 0$  and  $\ell \leq -2\sqrt{c/3}$  imply that

$$v(t) = -t^3 + \ell t + \frac{c}{t}$$

is monotone decreasing and convex for  $r < t < t_1 = \sqrt[4]{c/3}$  and  $v(t_1) \leq 0$ . It follows that  $t_0 \leq t_1$ , in particular.

Observe that  $f(t_0, \ell) = 0$ , and

$$f(t, \ell) = (\tau^2 - t^2) \left( -3 + \frac{c}{\tau^2 t^2} \right) \quad (26)$$

$$= \frac{3(\tau^2 - t^2)}{\tau^2 t^2} (a + \tau t)(a - \tau t), \quad (27)$$

where  $a = t_1^2 = \sqrt{c/3} \leq -\ell/2$ .

Since the first factors in (27) are positive for  $r \leq t < t_0$ , it is enough to show

$$\delta(t, \ell) = a - \tau t$$

is nonnegative for  $r \leq t \leq t_0$  and positive somewhere. Note that  $\delta(t_0, \ell) = a - t_0^2 \geq 0$  with strict inequality unless  $\ell = -2a$ .

From the equation (24) defining  $\tau = \tau(t, \ell)$ , we find

$$\tau_t = -\frac{v'(t)}{v'(\tau)},$$

and

$$(\tau + t) \left( \tau^2 - \tau t + t^2 - \ell - \frac{c}{\tau t} \right) = 0.$$

In particular,

$$\ell + \frac{c}{\tau t} = \tau^2 - \tau t + t^2. \quad (28)$$

On the other hand,

$$\begin{aligned} \delta_t &= -\frac{1}{v'(\tau)} [\tau v'(\tau) - t v'(t)] \\ &= -\frac{1}{v'(\tau)} (\tau - t) \left[ -3(\tau^2 + \tau t + t^2) + \ell + \frac{c}{\tau t} \right]. \end{aligned}$$

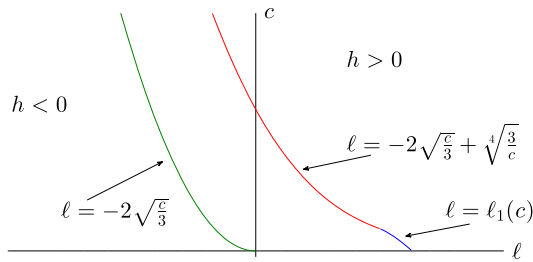


**Fig. 14.** Preliminary estimates locating the toroidal solutions.

Substituting from (28), we find

$$\delta_t = \frac{2}{v'(\tau)}(\tau - t)(\tau + t)^2.$$

Recall that  $v'(\tau) < 0$  and  $0 < r \leq t \leq t_0 \leq \tau$ . Thus,  $\delta_t \leq 0$  with equality only for  $t = t_0$ . It follows that  $\delta_t \leq 0$  and  $f(t, \ell) \geq f(t_0, \ell) \geq 0$  with strict inequality except when  $\ell = -2\sqrt{c/3}$  and  $t = t_0 = t_1$ .  $\square$

According to the results in this section, we understand the sign of the terminal heights for  $c > 0$  except in a relatively narrow strip containing the toroidal solutions. See Fig. 14.

### 3.4. Toroidal solutions

We now prove a conjecture formally appearing in [6] and building on past results of Gulliver [4] and Ross and Smith [11].

**Theorem 3.5.** *There is a single  $C^1$  curve in the  $(\ell, c)$  plane consisting of all solutions of the equation*

$$h(\ell, c) = 0. \tag{29}$$

*In particular, the rotational tori of equilibrium comprise a one parameter family of shapes.*

Our approach relies on various properties of the function  $h$  and its derivatives away from parameter values  $(\ell, c)$  for which  $|v| = |\sin \psi| = 1$  has double roots. We have already shown that  $h$  is continuous at such points in Lemma 3.1. In order to prove the conjecture, we will first need to strengthen this regularity assertion.

**Lemma 3.4.** *Assume  $r_0 = r_0(\ell_0, c_0)$  and  $R_0 = R_0(\ell_0, c_0)$  are simple zeros of the equation  $|v(t)| = 1$  and  $|v(t)| < 1$  for  $r_0 < t < R_0$ . Then the integral*

$$h = \int_r^R u'(t) dt$$

*is a  $C^1$  function of  $\ell$  and  $c$  in some open set about  $(\ell_0, c_0)$ .*

**Proof.** Changing variables in the integral by setting  $t = (1 - s)r + sR$  gives

$$h = (R - r) \int_0^1 u'((1 - s)r + sR) ds.$$

By direct calculation

$$\begin{aligned} \frac{\partial h}{\partial \ell} &= \frac{\partial(R-r)}{\partial \ell} \int_0^1 u'((1-s)r+sR) ds + (R-r) \int_0^1 \frac{\partial}{\partial \ell} u'((1-s)r+sR) ds \\ &= \frac{1}{(R-r)} \frac{\partial(R-r)}{\partial \ell} h + (R-r) \int_0^1 \frac{g(s)}{(1-v((1-s)r+sR))^2} ds, \end{aligned} \tag{30}$$

where

$$g(s) = \left( (1-s) \frac{\partial r}{\partial \ell} + s \frac{\partial R}{\partial \ell} \right) v'((1-s)r+sR) + (1-s)r+sR.$$

We also have

$$|\sin \psi(t)| = |v(t)| = 1$$

for  $t = r, R$ , so that

$$v'(r) \frac{\partial r}{\partial \ell} + r = v'(R) \frac{\partial R}{\partial \ell} + R = 0.$$

Therefore,

$$g(s) = (1-s)r \left( 1 - \frac{v'((1-s)r+sR)}{v'(r)} \right) + sR \left( 1 - \frac{v'((1-s)r+sR)}{v'(R)} \right).$$

By L'Hôpital's rule

$$\lim_{s \rightarrow 0} \frac{g(s)}{1-v((1-s)r+sR)} = \frac{1}{2v(r)v'(r)^2v'(R)} \left\{ rv'(R)v''(r) - \frac{Rv'(r)}{R-r}[v'(R) - v'(r)] \right\},$$

and

$$\lim_{s \rightarrow 1} \frac{g(s)}{1-v((1-s)r+sR)} = \frac{1}{2v(r)v'(r)v'(R)^2} \left\{ Rv'(r)v''(R) - \frac{rv'(R)}{R-r}[v'(R) - v'(r)] \right\}.$$

Since these limits are finite, we see the integral in (30) satisfies the hypotheses of Lemma 3.1.

Consequently, the integral in the expression for  $\partial h/\partial \ell$  is well defined and continuous. The same is true for  $\partial h/\partial c$  by very similar reasoning and the conclusion follows.  $\square$

### 3.5. Toroidal solutions with $c \leq 0$

We now study solutions of (29) in the half-plane  $c \leq 0$ . Our main assertion is the following:

**Proposition 3.1.** *For every  $c \leq 0$ , there is a unique value  $\ell^*(c)$  such that*

$$h(\ell^*(c), c) = 0.$$

Moreover,  $c \mapsto \ell^*(c)$  is a decreasing  $C^1$  function for  $-\infty < c < 0$ .

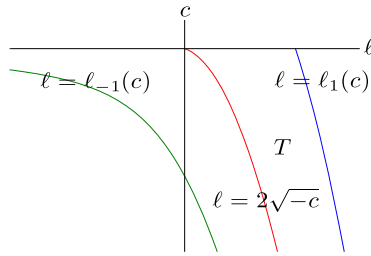


Fig. 15. The region  $T$ .

It is routine to verify that  $v(r_{\max}) \leq 0$  for  $\ell \leq 2\sqrt{-c}$ . This implies, using Lemma 3.2,

$$h(2\sqrt{-c}, c) < 0 \tag{31}$$

for  $c \leq 0$ . In particular, there are no pairs  $(\ell, c)$  with  $c \leq 0$  and  $\ell_{-1}(c) \leq \ell \leq 2\sqrt{-c}$  corresponding to toroidal solutions. Similarly, there are no pairs corresponding to toroidal solutions with  $c \leq 0$  and  $\ell \geq \ell_1(c)$ . See Lemma 4 of [6].

On the other hand,

$$\lim_{\ell \nearrow \ell_1(c)} h(\ell, c) = +\infty.$$

This is also shown in [6].

Accordingly, we restrict attention to the set

$$T = \{(\ell, c) : 2\sqrt{-c} < \ell < \ell_1(c), c \leq 0\}$$

indicated in Fig. 15. For each  $(\ell, c) \in T$ , the function  $v = \sin \psi$  has exactly two positive simple zeros  $0 < t_0 < t_1 < R$  and a unique maximum at  $r_{\max} \in (t_0, t_1)$ . Also, note that  $r$  and  $R$  are  $C^1$  in the interior of  $T$ , and so  $h$  is  $C^1$  in the interior of  $T$  by Lemma 3.4.

**Lemma 3.5.** Assume  $(\ell, c) \in T$ . Then

$$\frac{\partial h}{\partial \ell} = - \int_{[r, R] \setminus [t_0, t_1]} \left( \frac{t}{v'(t)} \right)' u'(t) dt + \int_{t_0}^{t_1} \frac{t}{(1 - v(t)^2)^{3/2}} dt \tag{32}$$

and

$$\frac{\partial h}{\partial c} = - \int_{[r, R] \setminus [t_0, t_1]} \left( \frac{1}{tv'(t)} \right)' u'(t) dt + \int_{t_0}^{t_1} \frac{1}{t(1 - v(t)^2)^{3/2}} dt. \tag{33}$$

**Proof.** Since

$$\frac{u''(t)}{(1 + u'(t)^2)^{3/2}} = v'(t), \quad t \in (r, R),$$

it follows that  $u'$  is strictly increasing on  $(r, r_{\max})$  and strictly decreasing on  $(r_{\max}, R)$ . Let  $w = (u')^{-1}$  be the inverse of  $u'$  restricted to  $(r, r_{\max})$ . Note that  $u''(w)w' = 1$ . Thus, introducing the variable  $\xi = u'(t)$ , we find

$$\int_r^{t_0} u'(t) dt = \int_{-\infty}^0 \xi w'(\xi) d\xi.$$

Similarly

$$\int_{t_1}^R u'(t) dt = \int_0^{-\infty} \xi w'(\xi) d\xi$$

where  $w$  denotes the inverse of  $u'$  restricted to  $(r_{\max}, R)$ .

In either change of variables,

$$v(w) = \frac{\xi}{\sqrt{1 + \xi^2}},$$

and it follows that

$$\frac{\partial w}{\partial \ell} = -\frac{w}{v'(w)}.$$

Thus

$$\begin{aligned} \frac{\partial}{\partial \ell} \int_{-\infty}^0 \xi w'(\xi) d\xi &= \int_{-\infty}^0 \xi \frac{\partial^2 w}{\partial \ell \partial \xi} d\xi \\ &= - \int_{-\infty}^0 \xi \frac{\partial}{\partial \xi} \left( \frac{w}{v'(w)} \right) d\xi \\ &= - \int_r^{t_0} \left( \frac{t}{v'(t)} \right)' u'(t) dt. \end{aligned}$$

Likewise, we find

$$\frac{\partial}{\partial \ell} \int_0^{-\infty} \xi w'(\xi) d\xi = - \int_{t_1}^R \left( \frac{t}{v'(t)} \right)' u'(t) dt.$$

Differentiating the equation

$$\frac{u'}{\sqrt{1 + u'^2}} = v$$

with respect to  $\ell$  gives

$$\frac{\partial u'}{\partial \ell} = t(1 + u'^2)^{3/2} = \frac{t}{(1 - v^2)^{3/2}}.$$

Since  $u'(t_0) = u'(t_1) = 0$ ,

$$\begin{aligned} \frac{\partial}{\partial \ell} \int_{t_0}^{t_1} u'(t) dt &= u'(t_1) \frac{\partial t_1}{\partial \ell} - u'(t_0) \frac{\partial t_0}{\partial \ell} + \int_{t_0}^{t_1} \frac{t}{(1-v(t)^2)^{3/2}} dt \\ &= \int_{t_0}^{t_1} \frac{t}{(1-v(t)^2)^{3/2}} dt. \end{aligned}$$

Finally, writing

$$h = \int_r^{t_0} u'(t) dt + \int_{t_0}^{t_1} u'(t) dt + \int_{t_1}^R u'(t) dt,$$

we have

$$\frac{\partial h}{\partial \ell} = - \int_r^{t_0} \left( \frac{t}{v'(t)} \right)' u'(t) dt + \int_{t_0}^{t_1} \frac{t}{(1-v(t)^2)^{3/2}} dt - \int_{t_1}^R \left( \frac{t}{v'(t)} \right)' u'(t) dt$$

which is (32).

Formula (33) is obtained similarly once we compute

$$\frac{\partial w}{\partial c} = - \frac{1}{wv'(w)}, \quad \text{and} \quad \frac{\partial u'}{\partial c} = \frac{1}{t(1-v^2)^{3/2}}. \quad \square$$

**Proof of Proposition 3.1.** Observe that

$$- \left( \frac{t}{v'(t)} \right)' = - \frac{t^2(3t^4 + \ell t^2 - 3c)}{(-3t^4 + \ell t^2 - c)^2} < 0$$

since  $\ell > 0$  and  $c \leq 0$ . As  $u'(t) < 0$  for  $t \in [r, R] \setminus [t_0, t_1]$ , we have  $\partial h(\ell, c)/\partial \ell > 0$  by formula (32).

In view of (31), we may conclude that for each  $c \leq 0$  there is a unique number  $\ell^* = \ell^*(c)$  such that  $h(\ell^*(c), c) = 0$  as asserted.

Next notice that

$$- \left( \frac{1}{tv'(t)} \right)' = \frac{-9t^4 + \ell t^2 + c}{(-3t^4 + \ell t^2 - c)^2}.$$

Since  $u'(t) < 0$  for  $t \in [r, R] \setminus [t_0, t_1]$ , it follows that  $tv = -t^4 + \ell t^2 + c < 0$  on  $[r, R] \setminus [t_0, t_1]$ . In turn,

$$-9t^4 + \ell t^2 + c < -t^4 + \ell t^2 + c < 0$$

on these same intervals. Hence,

$$- \left( \frac{1}{tv'(t)} \right)' u'(t) > 0$$

on  $[r, R] \setminus [t_0, t_1]$  and consequently,  $\partial h/\partial c > 0$  by formula (33).

It is now immediate that  $c \mapsto \ell^*(c)$  is  $C^1$  and decreasing. Indeed differentiating the equation  $h(\ell^*(c), c) = 0$  gives

$$(\ell^*)'(c) = - \frac{\partial h(\ell^*(c), c)}{\partial c} / \frac{\partial h(\ell^*(c), c)}{\partial \ell} < 0. \quad \square$$

### 3.6. Toroidal solutions with $c > 0$

We now consider solutions  $(\ell, c)$  of  $h(\ell, c) = 0$  for  $c > 0$ . The arguments above for  $c \leq 0$  do not easily extend to this case. Instead, we turn to an alternative pair of parameters introduced by Smith and Ross [11].

We have shown that all solutions with  $c > 0$  lie within the strip

$$\{(\ell, c) : -2\sqrt{c/3} < \ell < \min\{-2\sqrt{c/3} + \sqrt[4]{3/c}, \ell_1(c)\}, c \geq 0\}$$

with the usual convention that the minimum reverts to defined quantities. More generally, with  $\bar{A}$  denoting the closure of the set defined in (23), we consider the complement

$$S = \{(\ell, c) : c > 0\} \setminus \bar{A}.$$

For  $(\ell, c) \in S$ , the equation  $|v| = 1$  has only simple roots. In fact the equations

$$\begin{cases} v(r_1) = -r_1^3 + \ell r_1 + \frac{c}{r_1} = +1 \\ v(R) = -R^3 + \ell R + \frac{c}{R} = -1 \end{cases}$$

have *unique* solutions  $r_1$  and  $R$  with  $r_1 < R$ . In particular,  $h \in C^1(S)$ . Moreover, we can express  $\ell$  and  $c$  uniquely in terms of  $r_1$  and  $R$

$$\begin{cases} \ell = r_1^2 + R^2 - \frac{1}{R-r_1} \\ c = \frac{r_1 R}{R-r_1} - (r_1 R)^2 \end{cases}. \quad (34)$$

In particular, this implies that we may use  $r_1$  and  $R$  as parameters for  $h$  when  $(\ell, c) \in S$ .

Expressing  $v$  in terms of  $r_1$  and  $R$  allows us to write

$$p(t) := tv(t) = (t^2 - r_1^2)(R^2 - t^2) - \frac{t^2 - r_1 R}{R - r_1}.$$

And further changing variables to  $t = Rs$

$$\begin{aligned} p(Rs) &= R^4(s^2 - (r_1/R)^2)(1 - s^2) - R \frac{s^2 - (r_1/R)}{1 - (r_1/R)} \\ &= R \left\{ \mu(s^2 - \lambda^2)(1 - s^2) - \frac{s^2 - \lambda}{1 - \lambda} \right\} \\ &= Rq(s) \end{aligned}$$

where

$$\lambda := \frac{r_1}{R}, \quad \mu := R^3$$

and

$$q(s) := \mu(s^2 - \lambda^2)(1 - s^2) - \frac{s^2 - \lambda}{1 - \lambda}.$$

In particular, using the change of variables  $t = Rs$  in the integral defining  $h$  gives

$$h = \mu^{1/3} \int_{\lambda}^1 \frac{q(s)}{\sqrt{s^2 - q(s)^2}} ds.$$

Notice that the mapping  $(x, y) \mapsto (x/y, y^3)$  is a smooth bijection of  $\{(x, y) : 0 < x < y\}$  onto  $(0, 1) \times (0, \infty)$ . Thus, we may use  $\lambda$  and  $\mu$  as parameters for  $h$  when  $(\ell, c) \in S$ . Moreover, using (34) we can write  $(\ell, c)$  explicitly in terms of  $(\lambda, \mu)$ :

$$\begin{cases} \ell = (1 + \lambda^2)\mu^{2/3} - \frac{1}{1-\lambda}\mu^{-1/3} \\ c = \frac{\lambda}{1-\lambda}\mu^{1/3} - \lambda^2\mu^{4/3} \end{cases} \tag{35}$$

Some properties of the map  $(\lambda, \mu) \mapsto (\ell, c)$  we will quote later are detailed below. Also see Fig. 16 for reference.

**Lemma 3.6.** *Define  $(\ell, c)$  as in (35) and fix  $\lambda \in (0, 1)$ .*

- (i)  $\mu \mapsto \ell(\lambda, \mu)$  is strictly increasing.
- (ii)  $\lim_{\mu \rightarrow 0^+} \ell(\lambda, \mu) = -\infty$ .
- (iii)  $\lim_{\mu \rightarrow (\lambda(1-\lambda))^{-1}} \ell(\lambda, \mu) = (\lambda(1-\lambda))^{-2/3} - (\lambda(1-\lambda))^{1/3} \geq \ell_1(0) = 3/4^{1/3}$ .
- (iv)  $c(\lambda, \mu) > 0$  implies  $\mu < (\lambda(1-\lambda))^{-1}$ . We also have for  $(\lambda, \mu)$  such that  $(\ell, c) \in S$ :
- (v)  $\mu < (2\lambda(1-\lambda)^2)^{-1}$ , and
- (vi)  $\lambda \mapsto c(\lambda, \mu)$  is strictly increasing.

**Proof.** We only prove (v) as the assertions (i)–(iv) are simple to prove and (vi) follows from (v). If  $(\ell, c) \in S$ , then  $v'(r_1) < 0$ ; a routine computation shows  $v'(r_1) < 0$  is equivalent to (v).

The main reason for changing parameters as we have described above is indicated by the following monotonicity lemma which was established by Smith and Ross (see Lemma 3.2 and the appendix of [11]).

**Proposition 3.2.** *For each  $\lambda \in (0, 1)$ :*

- (i)  $(0, \infty) \ni \mu \mapsto h(\lambda, \mu)$  is increasing;
- (ii) there are values  $0 < \underline{\mu} \leq \bar{\mu} < \lambda/(1-\lambda)$  such that

$$h(\lambda, \underline{\mu}) \leq 0 \quad \text{and} \quad h(\lambda, \bar{\mu}) \geq 0;$$

- (iii) there is a unique value  $\mu = \mu^*(\lambda)$  such that  $h$  has a zero along the curve  $\mu \mapsto (\ell(\lambda, \mu), c(\lambda, \mu)) \in S$ .

We have established that all solutions of (29) for  $c \leq 0$  are in one-to-one correspondence with the points on the parameterized curve  $(-\infty, 0] \ni c \mapsto (\ell^*(c), c)$  and that all solutions of (29) for  $c > 0$  are in one-to-one correspondence with the points on the parameterized curve  $(0, 1) \ni \lambda \mapsto (\ell(\lambda, \mu^*(\lambda)), c(\lambda, \mu^*(\lambda)))$ . According to Lemma 3 of [4],  $\lim_{\lambda \rightarrow 0^+} (\ell(\lambda, \mu^*(\lambda)), c(\lambda, \mu^*(\lambda))) = (\ell^*(0), 0)$ . Consequently, these curves must meet at  $(\ell^*(0), 0)$  to form a single continuous curve.

All that remains is to show this curve is  $C^1$  across  $c = 0$ . To this end, we establish that  $h$  is  $C^1$  near  $(\ell^*(0), 0)$ . While this fact is not a corollary of Lemma 3.4 (since it turns out that  $r$  is not  $C^1$  across the line  $c = 0$ ), we will make use of the expressions for the derivatives of  $h$  computed in the proof of Lemma 3.4.

**Lemma 3.7.** *The terminal height  $h$  is a  $C^1$  function of  $\ell$  and  $c$  in a neighborhood of  $(\ell^*(0), 0)$ .*

**Proof.** Let  $D$  denote an open disk centered at  $(\ell^*(0), 0)$  of a radius chosen so small that  $D$  does not intersect the curves  $\ell = \ell_{-1}(c)$  and  $\ell = \ell_1(c)$ . First we show that  $r$  and  $R$  are continuous on  $D$ . Recall that

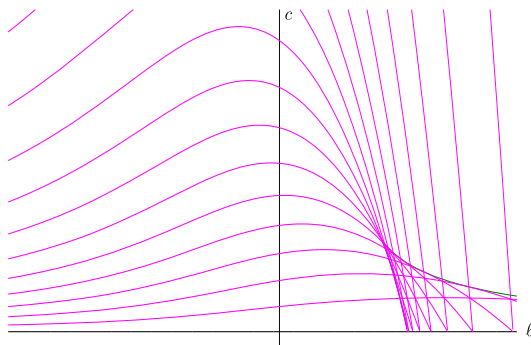


**Fig. 16.** Curves  $\mu \mapsto (\ell(\lambda, \mu), c(\lambda, \mu))$  for various  $\lambda \in (0, 1)$ .

on  $D \cap \{c < 0\}$ ,  $r = r(\ell, c)$  and  $R = R(\ell, c)$  are defined as the smaller and larger, positive solutions of the equation

$$v(t) = -t^3 + \ell t + \frac{c}{t} = -1,$$

respectively. Likewise, for  $D \cap \{c > 0\}$   $r(\ell, c)$  is defined as the unique solution of

$$v(t) = -t^3 + \ell t + \frac{c}{t} = +1$$

and  $R(\ell, c)$  is defined again as the unique solution of  $v(t) = -1$ . On  $D \cap \{c = 0\}$ , we define  $r(\ell, 0) = 0$  and  $R(\ell, 0)$  to be the unique positive solution of the cubic equation

$$-\rho^3 + \ell\rho = -1. \tag{36}$$

Implicit differentiation of the equation  $v(r) = -1$  in  $c$  gives  $\partial r/\partial c = -1/(rv'(r)) < 0$  and  $\partial R/\partial c = -1/(Rv'(R)) > 0$  on  $D \cap \{c < 0\}$ . As a result, the limits  $\lim_{c \nearrow 0} r = \rho_0$  and  $\lim_{c \nearrow 0} R = \rho_1$  exist; clearly  $0 \leq \rho_0 < \rho_1$ . If  $\rho_0 > 0$ , then we may pass to the limit in  $v(\rho_0) = -1$  to conclude  $\rho_0$  satisfies the cubic (36). However, this equation must also be satisfied by  $\rho_1 > \rho_0$ . As this cubic can only have one positive solution, it must be that  $\rho_0 = 0$  and  $\rho_1 = \rho$ .

Similarly, the limit  $\lim_{c \searrow 0} r = \varrho_0$  exists and must be zero. If  $\varrho_0 > 0$  then passing to the limit as  $c \searrow 0$  in  $v(r) = +1$  gives that  $\varrho_0$  satisfies

$$-\rho^3 + \ell\rho = +1.$$

As  $\ell < \ell_1(0)$ , the above cubic has no positive solution. Therefore,  $\varrho_0 = 0$  as claimed and  $\lim_{c \rightarrow 0} r = 0$ . It is easy to see we may also deduce that  $r$  tends to zero provided  $(\ell, c) \in D$  tends to a point on  $D \cap \{c = 0\}$ . Hence,  $r$  is continuous on  $D$ . Likewise, we can conclude  $R$  is also continuous on  $D$ .

Now let us study the derivatives of  $r$  and  $R$  across  $c = 0$ . From implicit differentiation and the fact that  $R$  tends to  $\rho > 0$  when  $c$  tends to 0, we can conclude that  $R \in C^1(D)$ . As for  $r$ , we explicitly compute for  $c \neq 0$

$$\frac{\partial r}{\partial \ell} = \frac{r^2}{4r^3 - 2\ell r + \frac{c}{|c|}}$$

and

$$\frac{\partial r}{\partial c} = \frac{1}{4r^3 - 2\ell r + \frac{c}{|c|}}.$$

By our comments above, we see that  $\frac{\partial r}{\partial \ell}$  tends to 0 for  $(\ell, c)$  tending to any point on  $D \cap \{c = 0\}$ . Hence,  $\frac{\partial r}{\partial \ell}$  is continuous across  $c = 0$ . Conversely,  $\frac{\partial r}{\partial c}$  tends to  $-1$  for  $(\ell, c) \in D \cap \{c < 0\}$  tending to any point on  $D \cap \{c = 0\}$ ; and  $\frac{\partial r}{\partial c}$  tends to  $+1$  for  $(\ell, c) \in D \cap \{c > 0\}$  tending to any point on  $D \cap \{c = 0\}$ .

As in Lemma 3.4, we compute

$$\begin{aligned} \frac{\partial h}{\partial c} &= \frac{\partial(R-r)}{\partial c} \int_0^1 u'((1-s)r+sR) ds + \\ &(R-r) \int_0^1 \frac{((1-s)\frac{\partial r}{\partial c} + s\frac{\partial R}{\partial c}) v'((1-s)r+sR) + \frac{1}{(1-s)r+sR}}{(1-v((1-s)r+sR)^2)^{3/2}} ds. \end{aligned} \tag{37}$$

Allowing  $(\ell, c) \in D \cap \{c < 0\}$  to tend to a point on  $D \cap \{c = 0\}$  in (37) gives

$$\begin{aligned} Q^- &= \left(\frac{\partial R}{\partial c} + 1\right) \int_0^1 u'(sR) ds + \\ &R \int_0^1 \frac{(-(1-s) + s\frac{\partial R}{\partial c}) v'(sR) + \frac{1}{sR}}{(1-v(sR)^2)^{3/2}} ds; \end{aligned}$$

and letting  $(\ell, c) \in D \cap \{c > 0\}$  to tend to a point on  $D \cap \{c = 0\}$  in (37) gives

$$\begin{aligned} Q^+ &= \left(\frac{\partial R}{\partial c} - 1\right) \int_0^1 u'(sR) ds + \\ &R \int_0^1 \frac{((1-s) + s\frac{\partial R}{\partial c}) v'(sR) + \frac{1}{sR}}{(1-v(sR)^2)^{3/2}} ds. \end{aligned}$$

Notice

$$\begin{aligned} \frac{R}{2} (Q^- - Q^+) &= R \int_0^1 u'(sR) ds - R^2 \int_0^1 \frac{(1-s)v'(sR)}{(1-v(sR)^2)^{3/2}} ds \\ &= \int_0^R u'(t) dt - \int_0^R \frac{(R-t)v'(t)}{(1-v(t)^2)^{3/2}} dt \\ &= \int_0^R u'(t) dt - \int_0^R (R-t)u''(t) dt \\ &= \int_0^R u'(t) dt - \left[ (R-t)u'(t) \Big|_0^R - \int_0^R \frac{d}{dt}(R-t)u'(t) dt \right] \\ &= \int_0^R u'(t) dt - \left[ -Ru'(0) + \int_0^R u'(t) dt \right] \\ &= 0. \end{aligned}$$

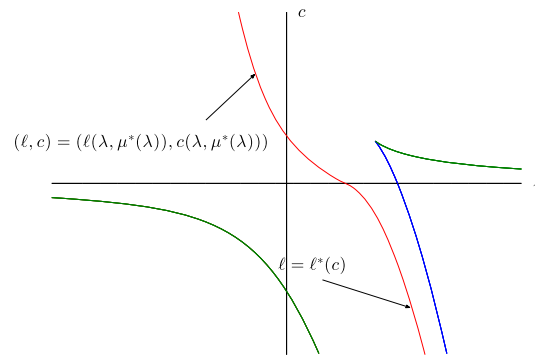


Fig. 17. The curve  $h(\ell, c) = 0$ .

Hence,  $\partial h/\partial c$  is continuous across  $D \cap \{c = 0\}$  and by Lemma 3.4, it is also continuous on  $D$ . An easier argument (simply employing formula (30)) can be made to show  $\partial h/\partial \ell$  is also continuous on  $D$ .  $\square$

In the proof of Proposition 3.1, we showed

$$\frac{\partial h(\ell^*(0), 0)}{\partial \ell} > 0.$$

By Lemma 3.7,  $h$  is continuously differentiable in a neighborhood of  $(\ell^*(0), 0)$ . Consequently, the curve of solutions of  $h(\ell, c) = 0$  must be  $C^1$  across  $c = 0$  by the implicit function theorem. As mentioned above, this is the final detail needed in the proof of Theorem 3.5.

We emphasize that while we have established the existence of a well-defined torus curve, we have not shown this curve is a graph  $\ell = \ell^*(c)$  for all values of  $c$  as shown in Fig. 17, though numerical computations indicate that this is the case.

## References

- [1] A. Beer, Note, Pogg. Ann. 96 (1855) 210.
- [2] R.A. Brown, L.E. Scriven, The shape and stability of rotating liquid drops, Proc. R. Soc. Lond. Ser. A 371 (1746) (1980) 331–357.
- [3] S. Chandrasekhar, The stability of a rotating liquid drop, Proc. R. Soc. Ser. A 286 (1965) 1–26.
- [4] R. Gulliver, Tori of prescribed mean curvature and the rotating drop, Soc. Math. de France, Astérisque 118 (1984) 167–179.
- [5] J. Heine, Computations of form and stability of rotating drops with finite elements, IMA J. Numer. Anal. 26 (2006) 723–751.
- [6] R. Hynd, J. McCuan, On toroidal rotating drops, Pacific J. Math. 224 (2) (2006) 279–289.
- [7] Nicolaos Kapouleas, Slowly rotating drops, Comm. Math. Phys. 129 (1990) (1990) 139–159.
- [8] R. López, Stationary rotating surfaces in Euclidean space, Calc. Var. Partial Differential Equations 39 (3–4) (2010) 333–359.
- [9] J.A.F. Plateau, Mémoire sur les phénomènes que présente une masse liquide libre et soustraite à l’action de la pesanteur, in: Mémoires de l’Acad. Bruxelles, vol. 16, 1843, pp. 1–35.
- [10] Lord Rayleigh, The equilibrium of revolving liquid under capillary force, Philos. Mag. Ser. 6 28 (164) (1914) 161–170.
- [11] D. Smith, J. Ross, Universal shapes and bifurcation for rotating incompressible fluid drops, Methods Appl. Anal. 1 (2) (1994) 210–228.
- [12] T.G. Wang, E.H. Trinh, A.P. Croonquist, D.D. Elleman, Shapes of rotating free drops: Spacelab experimental results, Phys. Rev. Lett. 56 (1986) 452–455.
- [13] H. Wente, The symmetry of rotating fluid bodies, Manuscripta Math. 39 (1982) 287–296.
- [14] N. Wilkin-Smith, A class of stable energy minimisers for the rotating drop problem, J. Math. Anal. Appl. 332 (2007) 577–606.